JOURNAL OF GEOPHYSICAL RESEARCH, VOL. 111, B11402, doi:10.1029/2005JB003632, 2006



# Restraining segments and reactivation of the Santa Monica–Dume–Malibu Coast fault system, offshore Los Angeles, California

Christopher C. Sorlien,[1] Marc J. Kamerling,[1,2] Leonardo Seeber,[3] and Kris G. Broderick[1,4]

Received 17 January 2005; revised 18 May 2006; accepted 3 August 2006; published 14 November 2006.

[1] A regional west striking system of surface and blind faults transects northern metropolitan Los Angeles, separating the Santa Monica Mountains from two deep sedimentary basins. The surface faults include the Santa Monica, Dume, and Malibu Coast faults. The three-dimensional (3-D) geometries of these faults and deformed dated strata were examined in order to determine how oblique shortening is accommodated, how structural relief grows along a mountain front, and how block translation is related to block rotation. Industry seismic reflection, well, and outcrop data were used to construct digital structure-contour maps of several of these faults and three stratigraphic horizons that intersect them. These maps, swath bathymetry, digital elevation models, and seismicity were incorporated into a 3-D digital database. Modeling included new approaches to determining strike-slip displacement by separate analyses of shortening and structural relief in a restraining double bend. Stratigraphic thicknesses indicate Miocene extension across the Santa Monica and Dume faults, which have been reactivated as a single or linked moderately dipping arcuate fault that accommodates one coherent block motion via left-lateral and left-reverse displacement. Modeling indicates 5 km (+8/−1 km) of left-lateral displacement on part of the Santa Monica–Dume fault and ~11° of clockwise rotation of the Santa Monica Mountains during the last ~4 ± 1 m.y. Modern displacement rates modeled from GPS data are similar to our modeled post-~4 Ma rates of westward escape and clockwise rotation of the Santa Monica Mountains.

**Citation:** Sorlien, C. C., M. J. Kamerling, L. Seeber, and K. G. Broderick (2006), Restraining segments and reactivation of the Santa Monica–Dume–Malibu Coast fault system, offshore Los Angeles, California, *J. Geophys. Res.*, *111*, B11402, doi:10.1029/2005JB003632.

## 1. Introduction

[2] Faults in continental crust commonly experience reactivation during successive tectonic phases and may inherit nonoptimum geometry for their current displacement directions [*Sibson*, 1995; *Scholz*, 2002]. This is the case along the southern and central California margin, which has experienced a changing tectonic regime following the cessation of subduction during early Miocene time [*Lonsdale*, 1991; *Atwater*, 1989, *Nicholson et al.*, 1994]. Regional Miocene extension and transtension were followed by post-Miocene shortening and transpression [*Crouch and Suppe*, 1993; *Wright*, 1991; *Clark et al.*, 1991]. Strike-slip faults are generally expected to be subvertical [*Anderson*, 1951]. Strike-slip motion can reactivate nonvertical faults that bend or are arcuate. These bends are three-dimensional; they are the intersections between two subplanar to curviplanar surfaces, and thus have a downdip dimension. Vertical displacement and extension/shortening occur across releasing/restraining domains between double bends of strike-slip faults [e.g., *Crowell*, 1974].

[3] Deformation of rocks is asymmetric across nonvertical strike-slip faults. Folds in the hanging walls of such faults trend at high angles to the faults [*Sorlien et al.*, 1999a] or subparallel to them [*Seeber et al.*, 2004; *Okay et al.*, 2004]. Relative to a fixed and little deforming footwall of a dipping North Anatolia continental transform, hanging wall rocks deform as they are transported by oblique slip through the transform's restraining and releasing segments [*Seeber et al.*, 2004; *Okay et al.*, 2004]. Uplift relative to the footwall accumulates as the hanging wall is transported through a restrained domain [*Shaw et al.*, 1994]. The eventual structural relief is thus the integral of the vertical component of its relative motion through the restrained domain. Thus, if the fault attitudes and relative vertical motions are known along a fault that contains three-dimensional (3-D) bends, then the slip can be modeled. Steeply dipping strike-slip faults, as exemplified by the Altyn Tagh fault in Tibet and the

[1]Institute for Crustal Studies, University of California, Santa Barbara, California, USA.
[2]Now at Venoco Inc., Carpinteria, California, USA.
[3]Lamont-Doherty Earth Observatory, Columbia University, Palisades, New York, USA.
[4]Now at ExxonMobil Exploration Co., Houston, Texas, USA.


0148-0227/06/2005JB003632$09.00

North Anatolia fault in Izmit Bay, Turkey, lack a consistent relative uplift pattern along restraining segments [*Cowgill et al.*, 2004; *Cormier et al.*, 2006].

[4] In spite of a century of intensive investigations of earthquake hazards along the southern California margin, fault 3-D geometry and kinematics are in some cases poorly known. Surprisingly, some of the least known faults are located directly offshore of Los Angeles. The Santa Monica and Dume faults dip beneath the mainland and also continue along strike beneath the city (Figure 1). These faults and others in this area of the offshore had only been mapped near the seafloor using single-channel seismic reflection data [e.g., *Junger and Wagner*, 1977]. Availability of migrated industry multichannel seismic reflection data allows us to produce digital 3-D representations of fault and stratal geometry, and then incorporate this geometry in three semi-independent modeling approaches. This modeling produced estimates of post- ~4 Ma kinematics, including translation, rotation, and vertical motion. Combinations of the different models produce a narrower range of slip and rotation estimates than would be the case for any single model.

[5] The 3-D geometry of faults and deformed dated strata record how oblique shortening is accommodated, how structural relief grows along a mountain front, and how block translation is related to block rotation. In particular, digital representations of this geometry allow us to model left-slip on a reactivated moderately dipping fault, with oblique slip rather than strain partitioning along a restraining segment. Such faults may be common where preexisting faults exist in nonoptimal orientations for later deformation. The relative importance of footwall subsidence versus hanging wall uplift to growth of structural relief [*Pinter et al.*, 2003], and how fault slip is dissipated into folding both along and across strike are also investigated.

## 2. Regional Tectonic and Structural Framework

[6] The southern California margin has experienced changing tectonic regimes. Pre-Neogene subduction produced large thrust faults that dip preferentially toward the north and east [*Legg*, 1991; *Sorlien et al.*, 1999a, 1999b; *Shaw and Suppe*, 1994; *Rivero et al.*, 2000]. Subduction ceased during early Miocene time, leading to extension as the Pacific plate obliquely diverged from the North American Plate [*Lonsdale*, 1991]. This motion and capture of part of the subducted slab by the Pacific Plate resulted in over 90° of Neogene clockwise rotation of the western Transverse Ranges (wTR) province [*Kamerling and Luyendyk*, 1979; *Nicholson et al*., 2004]. Removal of the wTR from its prerotation position alongside the Peninsular Ranges is related to large-scale Miocene extension and tectonic denudation of the Inner California Continental Borderland ("Inner Borderland"; Figure 1) as subduction-related thrusts were reactivated as (oblique) normal faults [*Yeats*, 1976; *Crouch and Suppe*, 1993]. This denudation explains the distribution of pre-Miocene rocks and exposure of the Catalina Schist accretionary rocks [*Crouch and Suppe*, 1993].

[7] Late Miocene changes of Pacific plate motion reduced extension across the transform boundary [*Cande et al.*, 1995; *Atwater and Stock*, 1998]. Most of the plate motion shifted from west of Baja California into the Gulf of California during early Pliocene time [*Atwater*, 1989]. That shift caused initiation of the southern San Andreas fault and produced the Mojave restraining double bend [*Crowell*, 1979]. The resulting north-south crustal shortening affected a wide area of the south central and southern California margin [*Clark et al.*, 1991; *Wright*, 1991; *Schneider et al.*, 1996; *Sorlien et al.*, 1999b; *Seeber and Sorlien*, 2000]. This shortening reactivated many of the large Miocene normal separation faults of the western Transverse Ranges and California Borderland as thrusts, oblique thrusts, and strike-slip faults. Mountains and islands grew as anticlinoria and represent inverted basins [*Davis et al.*, 1989; *Davis and Namson*, 1994; *Shaw and Suppe*, 1994, 1996; *Huftile and Yeats*, 1996; *Seeber and Sorlien*, 2000]. Many of the reactivated faults are arcuate, with strike changes of tens of degrees (Figures 1 and 2).

[8] This long history, including the more than 90° of Neogene clockwise rotation, resulted in an anomalous E-W trend for the western Transverse Ranges (wTR) province, which interrupts the regional NW-SE California structural grain. The Santa Monica Mountains are a southern part of the wTR (Figure 2). These mountains are separated from the basins to the south by active west striking faults, and by active folds above blind or partially blind faults. These faults include the Santa Monica, Dume, and Malibu Coast faults.

[9] Today, the San Andreas and the San Jacinto faults absorb more than half the dextral motion between the Pacific and North American plates. An additional 20% of the transform displacement is taken up by translation across NW striking right-slip faults that cut Los Angeles basin and the Inner Borderland (Figure 1). These faults separate basins from each other and terminate near the southern front of the wTR (Figure 2).

[10] Despite the substantial fault-normal convergence expected across the Mojave restraining segment of the San Andreas fault, it carries nearly pure right-lateral slip [*Yeats et al.*, 1996]. The convergent component is partitioned into belts of thrust or oblique-slip faults that strike west-northwest, nearly parallel to the local strike of the San Andreas fault. One system propagates and verges NNE into the Central Valley of California [*Keller et al.*, 2000] and another SSW toward the Pacific Ocean [*Keller and Loaiciga*, 1993]. The western Transverse Ranges is the south verging part of this system (Figure 1).

## 3. Tectonic Architecture of the Study Area

[11] The 70 km by 20 km study area lies offshore of the Santa Monica Mountains and includes Santa Monica Bay west to the Hueneme Fan area (Figure 2). It encompasses the structural and stratigraphic boundary between the Santa Monica Mountains and Santa Monica basin, including the west striking, Raymond-Hollywood–Santa Monica–Dume fault system (Figure 1) [*Dolan et al.*, 2000]. This fault system is now predominantly left-lateral with a strain accumulation rate of 2.4±1.1 mm/yr, according to a block model based on GPS data [*Meade and Hager*, 2005]. The onshore Malibu Coast and Santa Monica faults are probably oblique left-reverse faults [*Dibblee*, 1982; *Dolan et al.*, 2000]. NW striking right-slip faults terminate, split up, or

die out near the west striking fault system (Figure 2b) [*Yeats*, 2004; *Legg et al.*, 2004].

[12] The Santa Monica Mountains and Northern Channel Islands are the topographic expression of an east-west anticlinorium over 200 km long [*Bailey and Jahns*, 1954; *Davis and Namson*, 1994; *Shaw and Suppe*, 1994; *Seeber and Sorlien*, 2000]. Thrust slip on a low-angle blind fault beneath the Santa Monica–Dume fault is thought to account for the Santa Monica anticlinorium [*Davis and Namson*, 1994; *Dolan et al.*, 1995]. The Northern Channel Islands are folding during the late Quaternary [*Pinter et al.*, 2003], but active folding of the Santa Monica Mountains has not been demonstrated. In the structural and topographic saddle between the Santa Monica Mountains and Northern Channel Islands, the north limb of the anticlinorium has not tilted during late Quaternary time [*Seeber and Sorlien*, 2000;

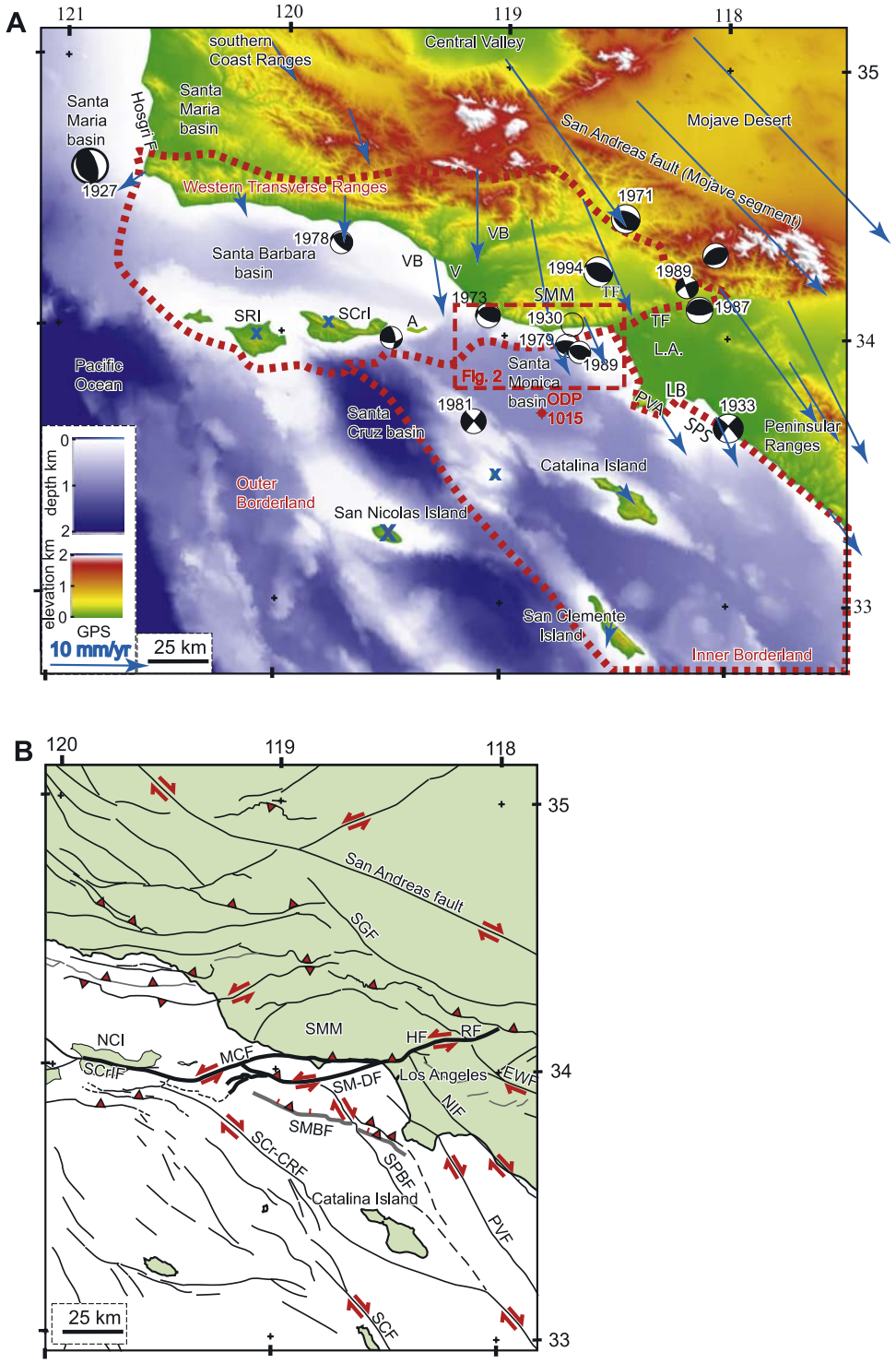


**Figure 1**

*Pinter et al.*, 2003]. Therefore the northern Channel Islands and the Santa Monica Mountains may fold independently today.

## 4. Methods

[13] The seismic reflection profiles located in Figure 2a were interpreted in order to map faults and stratigraphic horizons in 3-D. Lithologic information from petroleum test wells, seafloor outcrop, and published cross sections provided age control to quantify deformation rates and also to guide regional correlations through the seismic reflection data (Figures 3 and 4). These correlations revealed thickness changes as well as the missing section associated with unconformities. The resulting digital maps were visualized and modeled together with bathymetric, topographic, and seismicity data, using the 3-D software Gocad [e.g., *Mallet*, 1997]. The software UNFOLD was used for retrodeformation of the digital maps [e.g., *Gratier et al.*, 1999].

### 4.1. Data

[14] We used three overlapping ~2 km grids of 2-D industry multichannel seismic reflection data and regional profiles from two other data sets to map structure in 3-D and to correlate stratigraphy (Figure 2a). An additional 800 m × 2500 m grid of single-channel sparker and minisparker reflection data was used to map part of the San Pedro Basin fault trace. Data not shown in Figure 2 for clarity are described by *Burdick and Richmond* [1982]. A U.S. Geological Survey (USGS) single-channel 160 kJ sparker survey [*Moore and McCulloch*, 1975] was used along with sparse industry data to map the surface trace of the Santa Monica fault, offshore of Malibu (Figure 2b). Two of the industry grids covering the area west of the San Pedro Basin fault are migrated to 6 s TWTT, and they image acoustic basement as deep as ~4 s two-way traveltime (TWTT; Figures 5 and 6). Nonmigrated multichannel seismic reflection data from Digicon cover Santa Monica Bay between Point Dume and Palos Verdes Peninsula, along with USGS migrated multichannel seismic reflection profiles acquired in 1998 and 1999, using a small air gun and 250 m streamer [*Sliter et al.*, 2005]. Many of the USGS profiles are published [*Fisher et al.*, 2003; *Bohannon et al.*, 2004].

[15] Stratigraphic data provided the age control needed to examine evolution of faults and folds. All of the petroleum test wells in the offshore study area were drilled before 1970, and their logs are not available from the U.S. Minerals Management Service. Well data were available at the Long Beach office of the California Division of Oil and Gas and in files held at University of California, Santa Barbara, but not from every existing well (Figure 2a). Several of these wells were drilled in the hanging wall of the Santa Monica–Dume fault, including two with sonic logs (Figures 6 and 7; wells Shell CH-1 and Mobil 3490). The well information was converted to traveltime and correlated through the grids of reflection data, and around the east and west plunge of the Dume fault into the footwall basin to the south (Figure 5). Two wells located in the eastern offshore part of this footwall basin provided stratigraphic and paleontologic information (Figure 8, Standard 9R1 and Mobil SM-1). Stratigraphic correlations were supplemented by published information on seafloor outcrop [*Vedder*, 1990; *Nardin and Henyey*, 1978], by published cross sections that extend offshore [*Wright*, 1991], and by stratigraphic and velocity information from coastal and offshore oil fields at Playa del Rey and Venice Beach (Figure 3) [*California Division of Oil, Gas, and Geothermal Resources*, 1992; *Wright*, 1991].

### 4.2. Subsurface Mapping

[16] The seismic reflection profiles were jointly analyzed to construct structure-contour maps of three horizons: base Pliocene (which is the Miocene-Pliocene unconformity in part of the area), a horizon in the lower Pliocene, and a horizon in the upper Pliocene. Steep dips and thrust overlap are carefully represented on these digital 3-D horizon maps because these areas accommodate most of the shortening. Gently to moderately dipping faults can be directly imaged because the contrasting velocities and densities across them produce strong fault plane reflections. Other criteria for fault interpretation include the relationship of stratal folding to fault plane reflections (Figures 5 and 6), and truncations or offsets of stratal reflections (Figures 5 and 8). Faults were

**Figure 1.** (a) Topography, selected significant earthquakes, geographic localities, and GPS velocities (blue arrows) with respect to San Nicolas Island. The western Transverse Ranges (wTR) is the area of E-W structure outlined by the thick red dashed curve; another such curve outlines the Inner Borderland. GPS vectors selected from *Shen et al.* [2003] are corrected for the effects of large earthquakes but not modeled for locked faults. The crosses on islands indicate velocities too slow for arrows to be legible at this scale. Lower hemisphere earthquake focal mechanisms, labeled by year, are from *Scientists of U.S. Geological Survey and Southern California Earthquake Center* [1994], with location of 1930 earthquake (open circle) from *Hauksson and Saldivar* [1986]. Figure 2 is located by red dashed rectangle. A, Anacapa Island; L.A., Los Angeles (downtown); LB, Long Beach (city and harbor); PVA, Palos Verdes anticlinorium, peninsula and hills; SCrI, Santa Cruz Island; SMM, Santa Monica Mountains; SPS, San Pedro Shelf; SRI, Santa Rosa Island; TF, Tarzana Fan; V, Ventura; VB, Ventura sedimentary basin. The Northern Channel Islands anticlinorium underlies SRI and SCrI. (b) Surface or seafloor traces or upper edges of blind faults are from the Southern California Earthquake Center Community Fault Model (CFM) [*Plesch and Shaw*, 2002]. Blind faults are gray. Where CFM faults are not available, faults are from *Jennings* [1994] and this study. Paired arrows give sense of strike slip; triangles are on hanging walls of reverse-separation faults. EWF, Elsinore-Whittier fault; HF, Hollywood fault; MCF, Malibu Coast fault; NCI, Northern Channel Islands; NIF, Newport-Inglewood fault; PVF, Palos Verdes fault; RF, Raymond fault; SCF, San Clemente fault; SCrIF, Santa Cruz Island fault; SCr-CRF, Santa Cruz–Catalina Ridge fault; SGF, San Gabriel fault; SMBF, Santa Monica Bay fault; SM-DF, Santa Monica–Dume fault; SMM, Santa Monica Mountains; SPBF, San Pedro Basin fault.

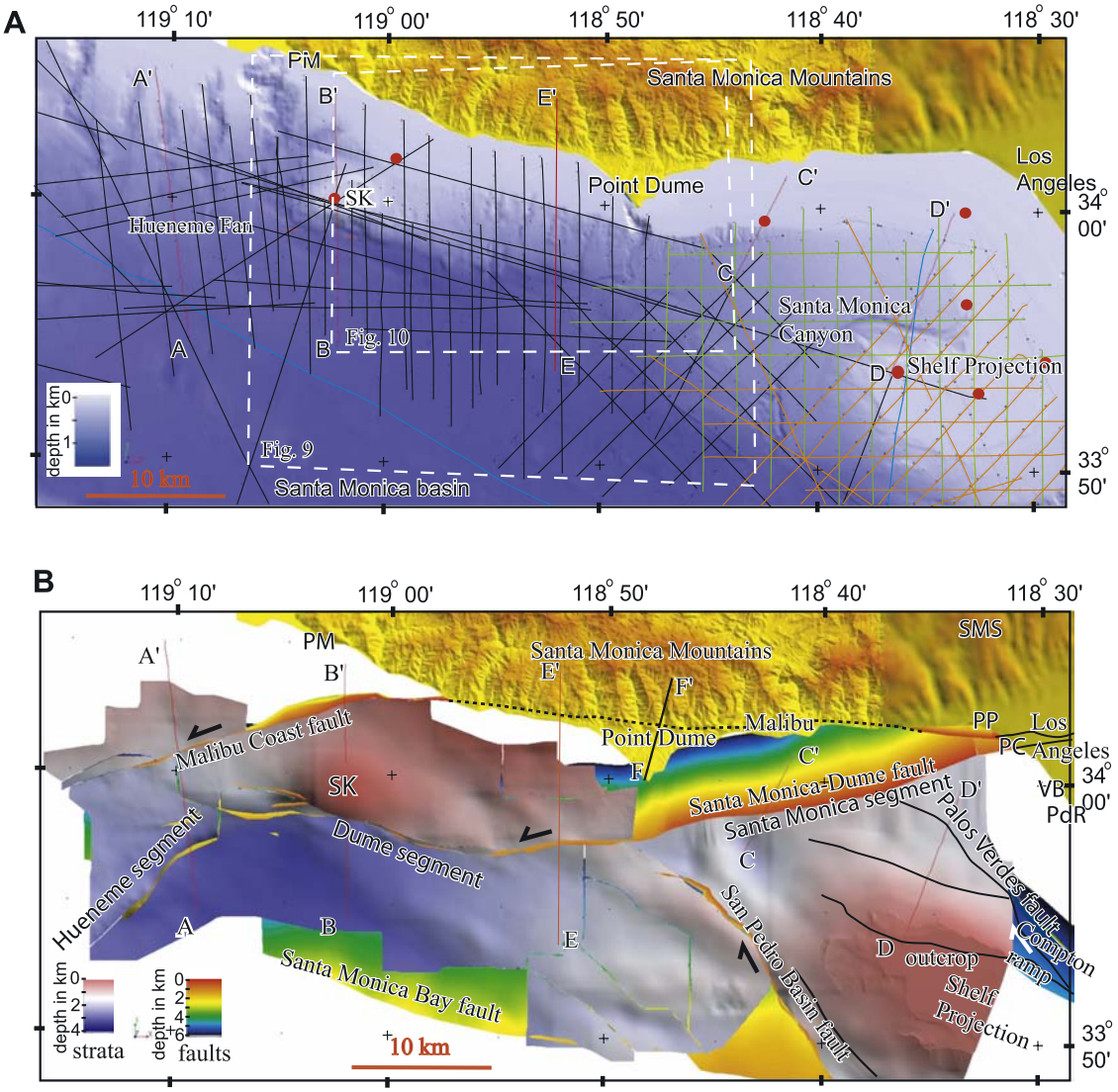


**Figure 2.** Plan views of Gocad model, located on Figure 1. (a) Profiles shown in Figures 4 (F-F′), 5 (A-A′), 6 (B-B′), 7 (C-C′), 8 (D-D′, 10A), 10C (E-E′) are located. Bathymetry, topography, tracks of multichannel seismic, and selected wells are indicated. Topography is a 30 m digital elevation model (DEM) west of 118°38′ and low-resolution topography from the SCEC Community Fault Model (CFM) east of there [*Plesch and Shaw*, 2002]. Bathymetry is regridded at 60 m from NOAA point data west of Point Dume and from USGS swath bathymetry east of Point Dume [*Dartnell and Gardner*, 1999]. Tracks of migrated industry seismic reflection profiles are black, nonmigrated Digicon profiles are green (not shown where not used in west), migrated USGS profiles are orange [*Sliter et al.*, 2005], and LARSE-2 and 3 plus USGS-125 are blue. Tracks of additional single-channel MMS and USGS seismic reflection data are shown by *Burdick and Richmond* [1982] and *Moore and McCulloch* [1975]. Red dots are those petroleum test wells for which we have stratigraphic information. (b) Offshore stratigraphic horizons and faults. Depth is given by the "strata" and "faults" legends. The horizon west of the San Pedro Basin fault is the ~4 Ma horizon (blue, or gray pattern, in Figures 5–8) and east of that fault, the base Pliocene (green, or gray pattern, in Figures 5–8) or seafloor in an area of Miocene outcrop is shown. Structural relief increases from east to west through the Dume segment because it is restraining for left-lateral displacement. Compton ramp and faults near Potrero Canyon are from SCEC CFM. PC, Potrero Canyon; PdR, Playa del Rey; PM, Point Mugu; PP, Pacific Palisades; SK, Sycamore Knoll; SMS, Santa Monica Slate outcrop; VB, Venice Beach.

then mapped in 3-D by tracing discontinuities and fault plane reflections through grids of intersecting industry seismic data. Interpretations were tested by correlation of strata on either side of faults, revealing large vertical separations across faults (Figure 6). Seafloor morphology from swath bathymetry is also locally helpful to confirm seafloor faults (insets to Figures 7 and 8). Seismicity was examined but not used in the construction of the fault

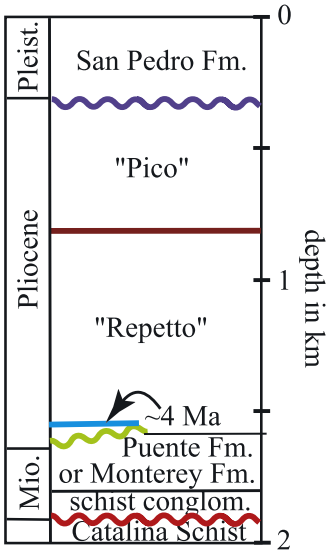


**Figure 3.** Stratigraphic column of depths from the Playa del Rey field, except San Pedro Formation, which is from the nearby offshore Venice field (both from *California Division of Oil, Gas, and Geothermal Resources* [1992]). Colors (or gray patterns) show our interpreted horizons, unconformities (wavy lines) are from our offshore interpretations, and schist conglomerate is shown a little thicker than is the case in the Playa del Rey field.

representations, and it is not shown in the figures. Instead, Animation S3 of cross section slices through the faults, folded strata, and seismicity was constructed and is included as part of auxiliary material data.[1]

[17] Interpolation and extrapolation of digital maps were done to ensure complete representations. The Santa Monica–Dume fault and the Santa Monica Bay fault were interpreted directly from the seismic profiles to, after depth conversion, as deep as 3 to 6 km near and west of Point Dume, and the offshore Malibu Coast fault was interpreted to 2.5 to 3 km depth. Structure-contour maps of faults and stratigraphic horizons were digitized in two-way traveltime, gridded, and converted to depth using a spatially variant velocity function. The bottom edges of faults were projected along dip in 3-D to either 6 km or 3 km because a smooth horizontal lower edge is needed for orientation in 3-D and map views. Because seismic reflection data over the eastern 10 km of the offshore Santa Monica fault were not available to us (Figure 2a), that fault was interpolated by joining, in Gocad, our representation at the edge of our data and the Southern California Earthquake Center (SCEC) Community Fault Model (CFM) representation at the coast (A. Plesch et al., Community fault model (CFM) for southern California, submitted to *Bulletin of the Seismological Society of America*, 2006] (see http://structure.harvard.edu/cfm/). The 45° dip interpreted to 1.2 km depth on C-C′ (Figure 7; corrected to depth) was projected to 6 km depth and used from that point east to the coast. The San Pedro Basin fault and other faults eastward could only be interpreted to 1 to 2 km depth. We mapped the Palos Verdes fault strands only at the seafloor because confident 3-D interpretations were not possible with the available data. Problems affecting interpretation of the Palos Verdes fault include multiple reflections on the U.S. Geological Survey data [*Sliter et al.*, 2005], nonmigrated industry data, and only tens of meters or less vertical separation for each fault strand in the upper few hundred meters.

### 4.3. UNFOLD and Map Restoration

[18] In order to quantify the strains due to faulting and folding, we restored the gridded structure contour maps of the lower Pliocene horizon to their undeformed state. The program UNFOLD assumes conservation of area and subhorizontal strata at the time of their deposition. UNFOLD organizes grid points of the digital maps into adjoining triangles, lays each triangle flat, and then minimizes gaps and overlaps among triangles in an iterative process [*Gratier et al.*, 1991, 1999; *Affolter and Gratier*, 2004]. This process yields maps of each flattened block between faults, which were then manually translated along faults and rotated to fit together using graphics software. The difference between restored and present positions and shapes of blocks defines the finite displacement field. We chose to represent the strain field relative to a reference line in a relatively stable area near the upper, inactive part of the Santa Monica Bay fault, and along the southern edge of data coverage. Rotations may be inferred during the fitting process; alternatively, rotations may be imposed on the restoration based on paleomagnetic or GPS data. The results include local estimates of shortening for each block and a regional displacement field derived from fitting all blocks by translation and rotation. Each choice has implications to other parts of the map, resulting in predictions for deformation.

## 5. Stratigraphy

### 5.1. Pre-Middle Miocene Sedimentary Rocks and Miocene Volcanic Rocks

[19] The Santa Monica–Dume–Malibu Coast fault system marks a sharp discontinuity in pre-middle Miocene stratigraphy between the Inner California Borderland and the western Transverse Ranges (Figures 1 and 2b). Cretaceous through early Miocene sedimentary rocks are underlain by the late Jurassic Santa Monica slate in the core of the Santa Monica Mountains anticlinorium [*Dibblee*, 1992]. In contrast, ''basement'' south of the Santa Monica–Dume fault is Mesozoic subduction-related Catalina schist, overlain directly by Miocene sedimentary or volcanic rocks (Figure 3) [e.g., *Vedder et al.*, 1986]. It is unclear whether the major prevolcanic lithologic boundary is located along the Malibu Coast fault or along the Santa Monica–Dume fault because geologic maps and cross sections, and wells for which we have data, do not penetrate beneath the volcanic rocks in the intervening Point Dume block (Figures 4, 6, and 7) [e.g., *Dibblee and Ehrenspeck*, 1993]. Miocene volcanic rocks dated at 17.4–16.3 Ma [*McCulloh et al.*, 2002; P. Gans, written communication, 19 October 2004] are typical of the Santa Monica Mountains and the Point Dume block. In contrast, these rocks are absent south of the Santa Monica–Dume fault

[1] Auxiliary materials are available in the HTML. doi:10.1029/2005JB003632.

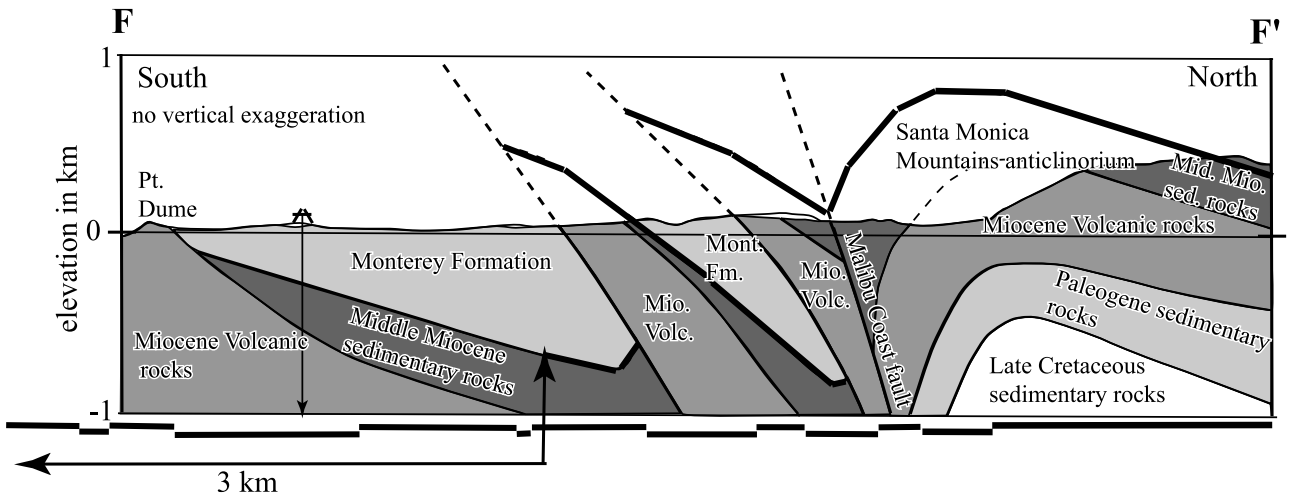


**Figure 4.** Cross section showing the Malibu Coast fault and subparallel faults and folded stratigraphy of the Santa Monica Mountains, located in Figure 2b. This is simplified from *Dibblee and Ehrenspeck* [1993]; faults and horizons are projected into the air. The line segments corresponding to near top middle Miocene sedimentary rocks are flattened to give shortening since the beginning of convergent block displacement. Significant shortening offshore southwest of this location initiated ~4 Ma, although shortening could have started here as early as ~5 Ma. Shortening from line length balancing is 3 km. This result assumes line length is conserved and is probably a minimum because of pressure solution and the conservative projection of the balanced horizon into the air.

where deep wells exist near and offshore Venice/Playa del Rey (Figures 2b and 3) [*Wright*, 1991].

[20] The Miocene volcanic rocks have higher density and interval velocity than do the overlying sedimentary rocks [e.g., *ten Brink et al.*, 2000], resulting in a strong acoustic impedance contrast and strong reflection. A high-amplitude reflection from the top of the Miocene volcanic rocks drilled on the hanging wall of the Santa Monica–Dume fault can be traced to volcanic rocks that crop out east of Anacapa Island (Figures 5 and 6) [*Vedder et al.*, 1986]. It can also be traced to 4 km depth beneath Santa Monica basin (Figure 5). The nature of the strata producing the reflection beneath Santa Monica basin is not known because of lack of well data. The reflection could be the top of Miocene volcanic rocks, coeval sedimentary rocks, or even top Catalina schist basement. An interval of high-amplitude reflections suggest that early Miocene rocks are present in the hanging wall of the Santa Monica Bay fault, and are largely absent in its footwall to its south (Figure 6).

### 5.2. Postvolcanic Miocene Rocks

[21] Middle and/or late Miocene Monterey Formation shale or the time-equivalent Puente Formation overlie volcanic rocks in the Santa Monica Mountains and Point Dume block. Beneath Santa Monica Bay, on the western Los Angeles structural shelf, and on Palos Verdes Hills and the offshore Shelf Projection (Figure 2), Monterey Formation overlies Miocene schist sandstone above Catalina schist basement, or lies directly on this basement (Figures 2b, 3, and 4) [*California Division of Oil, Gas, and Geothermal Resources*, 1992; *Dibblee*, 1982; see also *Blake*, 1991]. Postvolcanic Miocene strata drilled at Sycamore Knoll ("SK" on Figure 2b) downlap onto the deep reflection beneath the modern bathymetric basin. This reflection is thus an unconformity, at least locally angular, representing at least 10 million years of missing section (Figures 5 and 6).

### 5.3. Post-Miocene Strata

[22] Pliocene "Repetto," upper Pliocene–early Quaternary "Pico," and Quaternary undifferentiated strata (or Pleistocene San Pedro Formation) overlie the Miocene rocks (Figure 3). The Repetto and Pico intervals nearly correspond to the more modern use of "lower and upper Fernando Formation." However, Repetto and Pico terminology is used in this paper in an effort to be consistent with available well reports, published cross sections, and maps. Simply replacing the older names with Fernando Formation or with Repettian stage and Venturian stage ages might be erroneous as discussed by *Wright* [1991, p. 39]. We mapped and modeled a reflection within the lower part of the Repetto. Its age probably falls within the range for the onshore base Repetto unconformity (between 4.42 ± 0.57 m.y. and 3.4 ± 0.3 m.y.) [*Blake*, 1991]. This "~4 Ma horizon" was originally subhorizontal because the reflections beneath it are parallel and do not thin in the upthrown hanging wall of the western Santa Monica–Dume fault. The top Repetto is ~2.5 Ma in Los Angeles basin [*Blake*, 1991]. The base of up to 1 km thick late Quaternary strata of Hueneme Fan (Figure 2a) may be as young as a quarter of a million years, if the ~3 mm/yr post ~50 ka sedimentation rates of Ocean Drilling Program site 1015 can be extrapolated downward to a top Pico sequence boundary (Figure 5) [*Normark et al.*, 2004; W. Normark, verbal communication, September 2004]. The age of uppermost Pico is not directly known beneath Hueneme Fan but directly overlying strata are estimated at 0.9 ± 0.1 Ma locally in Los Angeles basin [*Tsutsumi et al.*, 2001]. Post-Pico strata are present and continuous east of the San

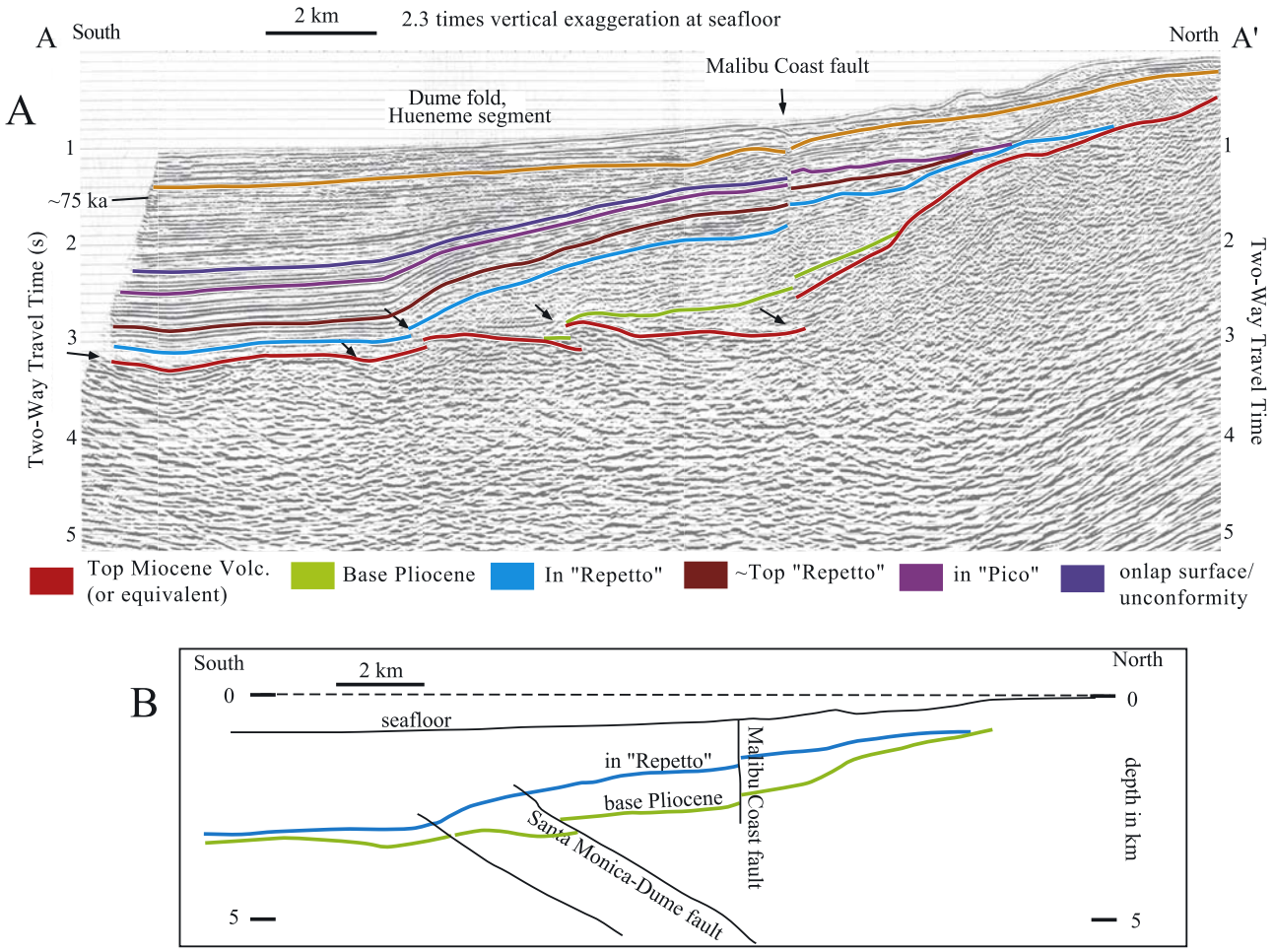


**Figure 5.** (a) Migrated multichannel seismic reflection (MCS) profile A-A′, located in Figures 1 and 2. This profile crosses the blind NE-SW Hueneme segment of the Santa Monica fault. Arrows are aligned along faults. The Malibu Coast fault is vertical in its upper 3 km. The shallowest interpreted horizon (orange or short gray dashes) is 0.1 s two way traveltime (less than 100 m) above horizon A from *Normark et al.* [1998], now estimated to be ~75 ka [*Normark et al.*, 2004]. We interpret the "violet" (or dark gray dashes) horizon labeled "onlap surface/unconformity" to be the top Pico and base of Hueneme Fan. (b) Cross section from the Gocad model along A-A′, without vertical exaggeration.

Pedro Basin fault, and are called the San Pedro Formation in the offshore Venice oil field (Figure 3).

## 6. Structural Interpretations

### 6.1. Fault Geometry in Map View

[23] Our new 3-D fault representations generally show greater continuity and connectivity, and in some cases strike differently, than the discontinuous 2-D fault traces shown on published maps [e.g., *Jennings*, 1994]. We mapped an ENE-WSW fault, roughly aligned with the onshore Santa Monica fault, across the shelf and slope east of Point Dume (Figure 7, inset). This fault connects directly through a bend with the WNW striking Dume fault (Figure 2b). Thus we refer to the Santa Monica–Dume fault as a single arcuate onshore-offshore fault. The Dume fault had previously been interpreted as distinct from the Santa Monica fault across a left step [*Hauksson and Saldivar*, 1986; *Dolan et al.*, 2000]. We mapped the WSW striking offshore Malibu Coast fault across Hueneme Fan to south of Anacapa Island, where it aligns with the Santa Cruz Island fault (Figures 1 and 2b). This differs from previous interpretations where a west striking Dume fault connected with the Santa Cruz Island fault, and the offshore Malibu Coast fault was not shown [*Junger and Wagner*, 1977; *Vedder et al.*, 1986]. The Malibu Coast fault splits from the Santa Monica–Dume fault near the coast at Pacific Palisades [*Dolan et al.*, 2000], and the two faults reconnect 60 km to the west via a set of distributed high-angle strands with small (tens of meters) vertical separation of Pliocene strata (Figure 2b).

[24] In addition to providing new maps of known faults, we constructed 3-D digital representations of blind faults that were previously unknown in the published literature. These include NW dipping faults along the Hueneme segment that splay from beneath the Santa Monica–Dume fault (Figures 2b and 5). Also included is a large north dipping fault, the Santa Monica Bay fault (formerly called the Shelf Projection blind fault by *Sorlien et al.* [2004], which we mapped offshore south

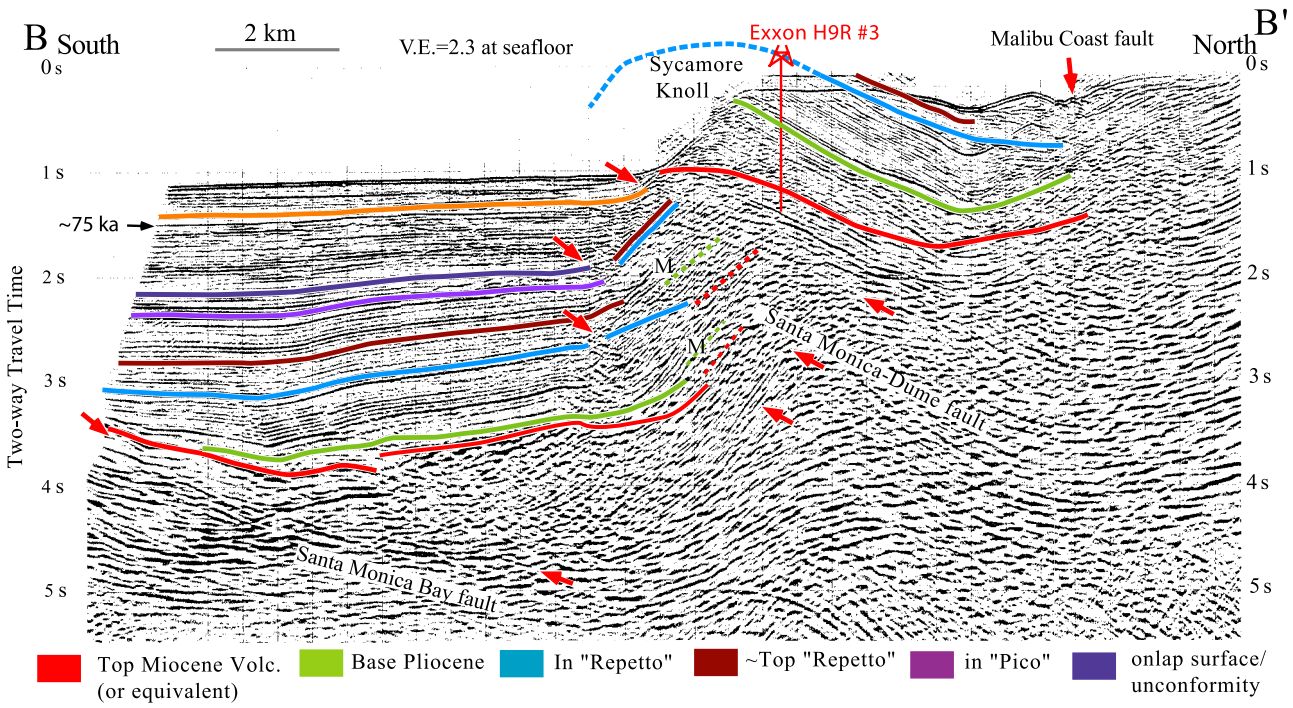


**Figure 6.** Migrated MCS profile B-B′, located in Figures 2, 9, and 10. Arrows are aligned along faults. Interpreted stratal horizons are the same as in Figure 5a. The interval between top Miocene volcanics and base Pliocene horizon is thicker in the upthrown hanging wall of the Santa Monica–Dume fault than in the footwall, indicating basin inversion. Although there is almost no deformation of Pliocene strata above the upper part of the Santa Monica Bay fault, folding of the Santa Monica Mountains may be related to blind slip on the deeper downdip fault. M, multiple reflection. A cross section along B-B′ through the Gocad depth model is presented in Figure 10.

of and beneath the Santa Monica–Dume fault and which projects beneath the Santa Monica Mountains (Figures 2b, 6, 9, and 10). West of the San Pedro Basin fault, the Santa Monica Bay fault preserves normal separation of Miocene strata and its southern upper part has only been lightly and locally reactivated by Pliocene shortening (Figure 6).

### 6.2. The 3-D Geometry of Faults and Folds

[25] The Santa Monica–Dume fault exhibits a broad range in the intensity of folding, the amount of thrust overlap, and the magnitude of structural relief across it (Figures 9 and 10). The variation of this deformation is systematically associated with changes in strike of this fault, whereas the dip remains fairly constant (40–50° north) in its upper 4–6 km (Figures 6, 7, 9, and 10). We subdivide this fault into three segments: the ENE striking Santa Monica segment, the WNW striking Dume segment, and the partially blind NE striking Hueneme segment (Figure 2b). A profile through the Shell CH-1 well and across the Santa Monica segment displays relatively little structural relief or thrust-repeated strata (Figure 7). In contrast, the Dume segment has much increased shortening and structural relief (Figure 6). Shortening is represented both by repeated strata across the fault and by folding at the culmination of the hanging wall anticline, which plunges abruptly west and more gradually to the east (Figure 9). A-A′ crosses the Hueneme segment, where NW dipping blind faults are associated with a set of subdued folds superposed on a regional south dipping fold limb or monocline (Figure 5).

[26] The Malibu Coast fault strikes ENE in the offshore area south and west of Point Mugu (Figure 2), cutting the hanging wall of the Dume fault. It is vertical above the top Miocene volcanics (or equivalent) reflection near and west of longitude 119°10′ (Figure 2), where it has about 200 m of north side-up separation at the ~4 Ma horizon and about 400 m at the top Miocene volcanics reflector. The onshore Malibu Coast fault dips steeply north (Figure 4) [*Dibblee and Ehrenspeck*, 1993]. A different set of high-quality industry seismic reflection data across the Dume segment and the Malibu Coast fault is shown by *Fisher et al.* [2005].

[27] The geometry of NW-SE right-slip faults is also represented, including the upper 1 to 2 km of the northern San Pedro Basin fault, and the seafloor traces of the Palos Verdes fault (Figures 2b, 8, 9, and 10). The shallow northern part of the San Pedro Basin fault is subvertical, and the magnitude and sense of vertical separation changes both along strike and by age of the offset horizon [*Sorlien et al.*, 2004; *Broderick*, 2006]. The northern Palos Verdes fault bends westward and branches into multiple WNW striking faults (three are mapped in Figure 2b). The expression of these branching strands progressively weakens toward the northwest and may terminate before reaching the Santa Monica–Dume fault. Northern strands of the Palos Verdes

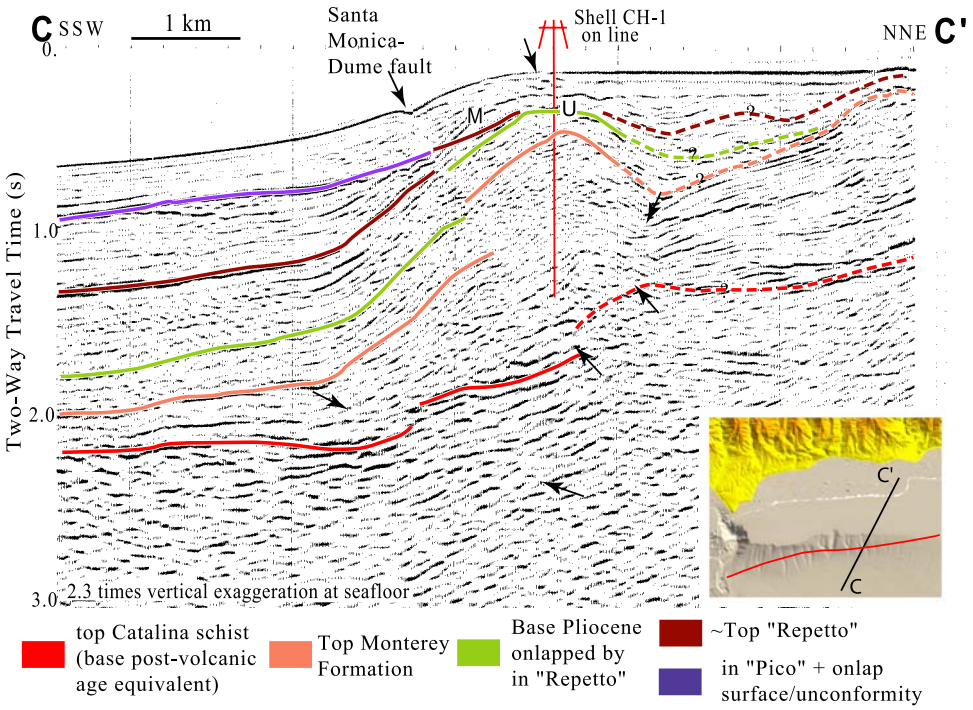


**Figure 7.** Migrated MCS profile C-C′, located in Figure 2 and inset. The left-lateral, 45° north dipping Santa Monica fault cuts halfway up the fold limb, and strata record little shortening near it. Like in Figure 6, thicker Miocene strata in the upthrown hanging wall north of the Santa Monica–Dume fault than in its footwall is consistent with basin inversion. The interval between the purple "in Pico" horizon and the violet (or gray patterns) "top Pico" unconformity/onlap surface, as well as the lower part of Hueneme Fan, have pinched out. Thus the section above violet is likely late Quaternary. M, multiple reflection; U, unconformity. The inset shows the 30 m DEM and 16 m gridded multibeam bathymetry [*Dartnell and Gardner*, 1999]. The seafloor trace of the Santa Monica–Dume fault, mapped using seismic reflection profiles, is the red or black curve.

fault display only tens of meters of vertical separation of the ~2.5 Ma top Repetto horizon (Figure 8).

## 7. Discussion

### 7.1. Stratigraphic Evidence for Post-Miocene Basin Inversion and Regional Subsidence

[28] The distribution and thickness of Miocene rocks support a Miocene extensional or transtensional history across north dipping faults, which may have originated as subduction-related thrust faults. Middle and late Miocene strata are thick in the upthrown hanging wall of the Santa Monica–Dume fault, and are thin or missing in the footwall (Figures 3, 4, and 6). Early Miocene sedimentary and volcanic rocks are kilometers thick in the western Santa Monica Mountains, whereas a relative lack of reflections beneath the strong base Pliocene reflection suggests early Miocene rocks are thin beneath the adjacent part of Santa Monica basin. Catalina Schist basement is present directly beneath Middle Miocene sedimentary rocks in wells drilled in the footwall of the Santa Monica fault near Playa del Rey and offshore Venice (Figure 3) and along D-D′ (Figure 8). This relation can be explained by early Miocene tectonic denudation and erosion, followed by subsidence.

[29] Plio-Quaternary strata are thickest where the Miocene strata are thinnest, consistent with basin inversion due to transpressional post-Miocene reactivation of the Santa Monica–Dume fault [*Schneider et al.*, 1996; *Seeber and Sorlien*, 2000]. The thickest post-Miocene strata (Repetto, Pico and San Pedro intervals) are located in a trough centered 5 km south of the onshore Santa Monica fault (Figures 2b and 8) [*Wright*, 1991; *Tsutsumi et al.*, 2001; see also *Bohannon et al.*, 2004]. This post-Miocene footwall basin continues offshore as far west as the San Pedro Basin fault near Point Dume (Figures 7, 8, and 10).

[30] The Miocene-Pliocene unconformity represents nondeposition or erosion of strata spanning millions of years. The hiatus is longest in the footwall of the Santa Monica Bay fault, where all of the Miocene and part of the early Pliocene strata are thin or missing. The lack of Miocene rocks can be explained by subaerial and wave erosion on a highstanding footwall block. Probable lack of Cretaceous and Paleogene rocks can be explained by tectonic denudation of the footwall. The Santa Monica Bay fault is thus a former low-angle normal separation fault that is part of the detachment system responsible for both the Miocene part of clockwise rotation of the western Transverse Ranges, and for tectonic denudation of the Inner Borderland [e.g., *Crouch and Suppe*, 1993].

[31] The Miocene-Pliocene angular unconformity is probably wave-eroded because it is planar and represents 10 million years or more of missing strata (Figures 5 and 6).

The present maximum depth of the unconformity is 4 km (near longitude 119°05′; Figure 2b), which would require an average subsidence rate of 0.8 mm/yr since 5 Ma. The adjoining northern Santa Cruz basin (Figure 1) has also subsided ~4 km since crustal shortening commenced [*Pinter et al.*, 2003]. The Miocene-Pliocene angular unconformity contrasts with the top Pico sequence boundary, which also represents a missing stratal interval. Most of the missing section represented by the younger sequence boundary is due to onlap rather than to deep erosion, and there is no requirement that it was affected by wave erosion.

### 7.2. Post-Miocene Kinematics

#### 7.2.1. Vertical Motions and Blind Thrust Slip

[32] Structural relief may increase across a mountain front in several ways, including by reverse slip on surface faults, by oblique slip in restraining segments of strike-slip faults, and by folding above blind thrust faults. Near the western terminus of the Santa Monica Mountains, near B-B′, a reverse slip component on the Dume segment and folding close to this fault account for most of the relief (Figures 9 and 10). Vertical displacements across the Santa Monica–Dume fault are not consistent with the west plunge of the

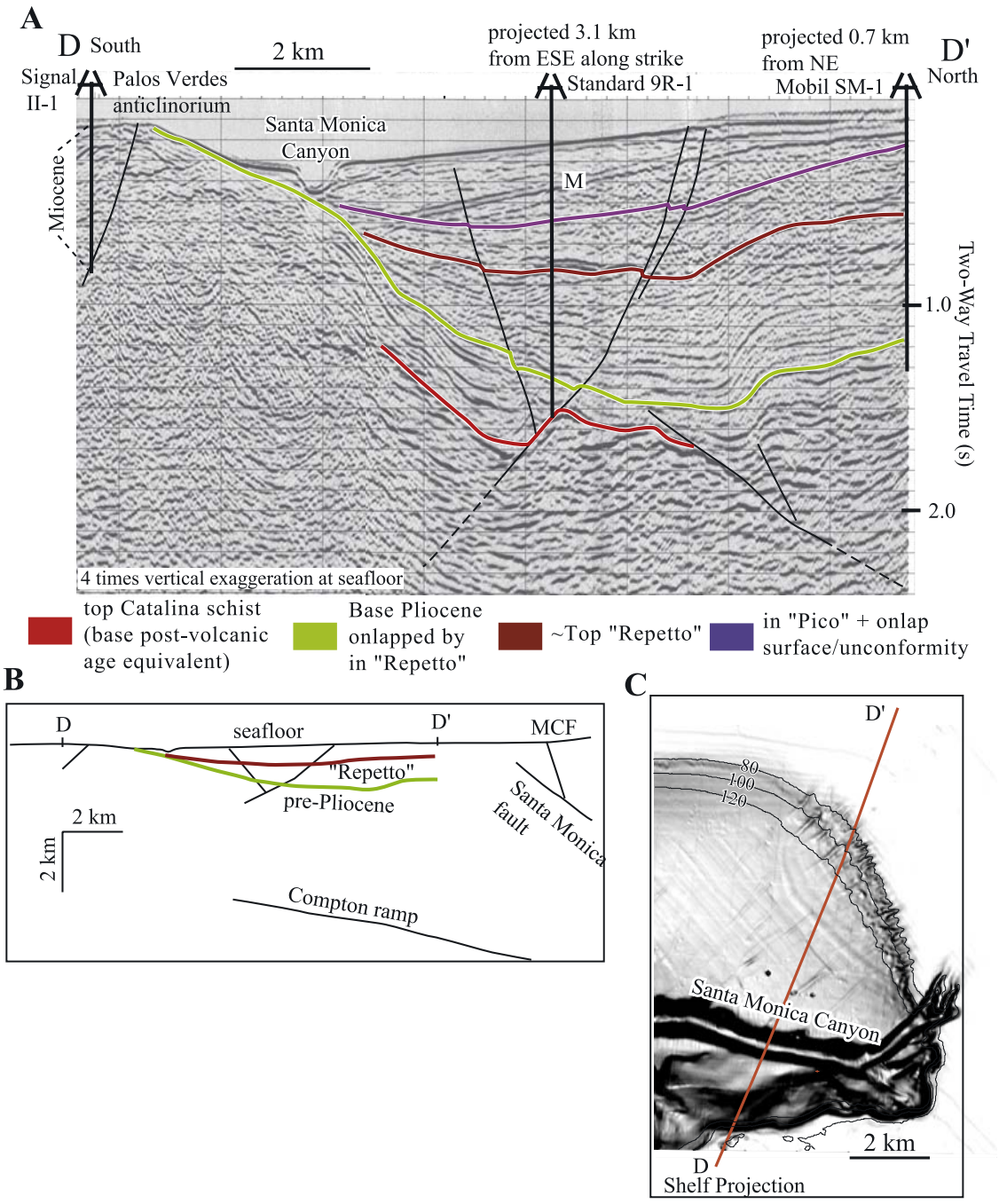


**Figure 8**

anticlinorium, however, and are not consistent with the fact that its core (''SMS'' in Figure 2b) is tens of kilometers east of the restraining Dume segment. Tilting of a broad, south dipping fold limb or homocline, rather than displacement on the shallow Santa Monica–Dume fault, created the relief south of Point Dume (Figure 10c). Part of that homocline along E-E′ is south of and beneath the Santa Monica–Dume fault. If deep displacement on a low-angle fault diminishes updip, then it creates a broad forelimb in the hanging wall [*Sibson*, 1995; *Sorlien et al.*, 2004]. Therefore tilting may be the result of blind thrust displacement on the underlying Santa Monica Bay fault. The west plunge of the Santa Monica Mountains anticlinorium may thus be the result of this blind thrust displacement increasing from west to east. Increased shortening and structural relief from west to east across the Malibu Coast fault (compare Figure 4 to Figure 5) also contributes to this west plunge between outcrop of Santa Monica slate (Figure 2b) and an offshore structural saddle 20 km east of Anacapa Island (Figure 1a).

[33] The Santa Monica Bay fault is a major fault (Figure 2b), but it is difficult to prove whether or not it has been active during Quaternary time. Post-Miocene strata are scarcely deformed above its upper part (Figures 6, 9, and 10); however, blind thrust displacement may exist on deeper parts of that fault, beneath the Santa Monica–Dume fault. The Santa Monica Bay fault projects downdip toward a basal thrust of *Namson and Davis* [1992, cross section 7, http://www.davisnamson.com/downloads/index.htm], renamed the Santa Monica Mountains thrust by *Dolan et al.* [1995]. The Santa Monica Bay fault, the Santa Monica–Dume fault, and the Malibu Coast fault all project in 3-D to the hypocenters of the oblique-reverse 1973 $M_L$6.0 Point Mugu earthquake, its aftershocks, and other earthquakes (Figure 1 and Animation S1 in the auxiliary material) [*Stierman and Ellsworth*, 1976; *Sorlien et al.*, 2003, Figure 3].

[34] Quaternary activity of the Santa Monica Bay fault and/or deep parts of the Santa Monica–Dume fault is implied by growth of structural relief, taking into account basin subsidence. Assuming the Miocene-Pliocene unconformity is wave-eroded beneath Santa Monica basin, the average post-Miocene rate of subsidence is 0.8 mm/yr. The downthrown footwall of the Malibu Coast fault near Point Dume exhibits slow surface uplift of marine terraces [*Birkeland*, 1972]. Little relative vertical displacement has occurred close to the shallow Santa Monica–Dume fault south of Point Dume. Tilting of the south limb of the Santa Monica Mountains anticlinorium is one explanation for a subsiding basin and uplifting Point Dume. This tilting would consume blind thrust displacement on the deep Santa Monica Bay fault (Santa Monica Mountains thrust) and/or deep parts of the Santa Monica–Dume fault. *Meigs et al.* [1999] interpret historic denudation rates to be similar to rates of post-Miocene increase in structural relief. Regional subsidence due to tectonic loading is not required for the edges of the anticlinorium in their model. We proposed that tectonic loading and postrift cooling do result in subsidence of the footwall south of the Santa Monica–Dume fault, and that crustal thickening is required to permit uplift of the coastline.

#### 7.2.2. Qualitative Discussion of Strike-Slip on Nonvertical Faults Between 3-D Bends

[35] Our fault and stratigraphic 3-D representations allow displacements to be modeled. In particular, the moderate dip of the Santa Monica–Dume fault results in a systematic relation between fault attitude and structural relief. The simple model in Figures 9b–9d shows the component of structural relief due to oblique reverse-left-lateral slip across the upper part of a planar restraining segment. Relative to a fixed footwall, if strike slip is greater than the length of the restraining segment, the greatest structural relief will be present at and beyond the downstream end of that segment (Figure 9d) [*Seeber et al.*, 2004]. For strike-slip motion that is half the length of the restraining segment, cumulative structural relief is constant over the downstream half of that segment (Figure 9c).

[36] Oblique slip in restrained domains bounded by moderately dipping faults is one of three main ways space problems are accommodated. In areas of transpression, a ''positive flower structure'' may form, where parallel-striking oblique-slip faults steepen and merge with depth [*Sylvester*, 1988; *Harding*, 1990]. Alternatively, oblique shortening may be accommodated by slip partitioning, where lower-angle thrust faults strike subparallel to shallow subvertical strike-slip faults, commonly with the faults merging into a steep oblique-slip fault at depth [e.g., *Lettis and Hanson*, 1991].

[37] The Santa Monica–Dume fault has a coherent relationship between fault geometry, slip direction, and growth of structural relief. The fault itself is arcuate and dips moderately to the north. On the basis of observations of structural relief of the ~4 Ma horizon on either side of it, we observe maximum shortening across the WNW striking

**Figure 8.** (a) Migrated MCS profile D-D′, located in Figures 2 and 8c. The sedimentary basin whose axis is seen in the middle continues with similar stratigraphy to the Playa del Rey and Venice Beach oil fields near the coast (Figures 2b and 3). The south flank of the basin is the progressively tilted north limb of the Palos Verdes anticlinorium. The near-seafloor faults are strands of the Palos Verdes fault. The blind north dipping fault strikes E-W and is linked to the anticline above it. This profile is shown with greater vertical exaggeration than Figures 5, 6, and 7. Standard 9-R1 bottoms in Catalina schist. (b) Cross section through our Gocad model centered on D-D′, with no vertical exaggeration. The seismic profile in Figure 8a ends at D′, south of the Santa Monica–Dume fault. The Santa Monica fault and Compton ramp are from the Southern California Earthquake Center Community Fault Model [*Plesch and Shaw*, 2002]. MCF, Malibu Coast fault. (c) Slope (gradient) map derived from 16 m grid of multibeam bathymetry (80, 100, and 120 m contours are labeled). Data are from *Dartnell and Gardner* [1999], and image is courtesy M.-H. Cormier. The northeastern, SW dipping strand of the Palos Verdes fault intersects the seafloor a few hundred meters south of the shelf break, along an alignment of disrupted seafloor ravines extending north from Santa Monica Canyon. A possible wave-cut platform from the Last Glacial Maximum is apparent that slopes southeast from ~90 m depth to between 100 and 120 m depth. Slope changes associated with a paleoshoreline could deflect ravines in addition to or instead of fault offset.

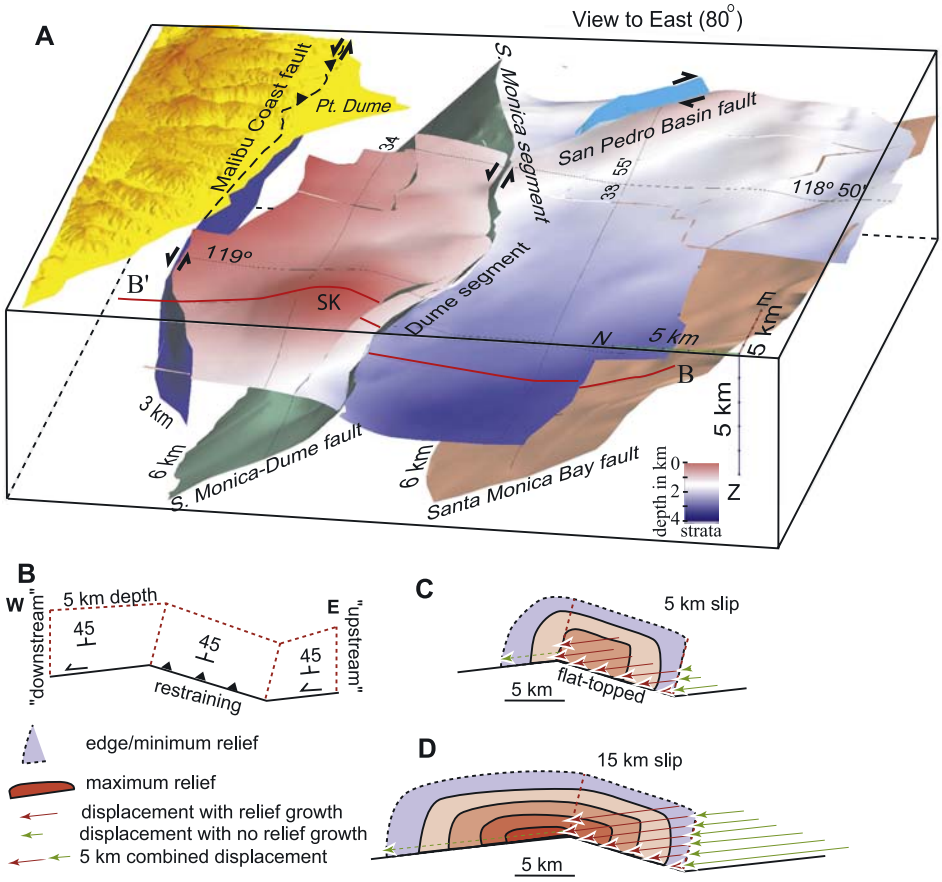


**Figure 9.** (a) Oblique view eastward (toward 80° azimuth), from 20° above horizontal, of the ~4 Ma horizon, faults (labeled), and the 30 m DEM. The position of B-B′ (Figure 6) is shown at its intersection with the ~4 Ma horizon. Folding of Sycamore Knoll (SK) is due to the Dume segment being restrained for left-lateral displacement. The farther rocks in the hanging wall (north) are transported through the restraining segment, the greater the structural relief. (b) Plan view of simplified but to scale model of the Dume restraining segment. The fault is only represented in its upper 5 km in this model; we do not mean to imply that it actually flattens below 5 km, nor are the actual fault segments planar and connected by such sharp kinks. (c) Qualitative growth in structural relief due to 5 km of left-lateral displacement parallel to the east striking parts of the fault. Structural relief only grows above the upper 5 km of the WNW striking restraining segment of the fault in this model. Vertical displacement is lacking above the west striking parts of the fault because the hanging wall is moving parallel to the strike and is neither moving up nor down the fault (green arrows). Structural relief increases above the restraining segment because the hanging wall is moving obliquely up the fault (red arrows). Contours indicate cumulative relief; deeper reds have larger relief. Cumulative relief increases through the "upstream" (eastern) 5 km of the restraining segment. The western 5 km of the restraining segment has a constant cumulative relief because rock there has been moving obliquely up the fault for the entire 5 km slip history. Relief decreases west of the restrained segment because it has spent successively less of its slip history moving obliquely up the fault along the restrained segment. (d) Same as Figure 9c except with 15 km displacement, which is longer then the 10-km-long restrained segment. Paired solid green and red arrows total 15 km in length. Cumulative slip increases westward through the entire restraining segment. The maximum relief continues 5 km west of the restraining segment because the hanging wall moved obliquely upward as it was transported through the entire 10 km of the restraining segment.

Dume segment, and minimum shortening across the offshore ENE striking Santa Monica segment (Figures 2b, 9a, and 10). The simplest explanation for these observations is left-lateral displacement parallel to the Santa Monica segment causing the hanging wall to override the restraining Dume domain.

[38] The Malibu Coast fault also exhibits shortening on one side of a bend. Little structural relief or shortening is present across the subvertical ENE striking Malibu Coast fault across Hueneme Fan (Figure 5), whereas its E-W segment along the Santa Monica Mountains dips north and has large structural relief and component of shortening (Figure 4), which steepened and overturned the Monterey Formation [*Dibblee*, 1992, 1993; *Dibblee and Ehrenspeck*, 1993]. The Dume segment and the onshore Malibu Coast fault form mirror image restraining segments, with shorten-

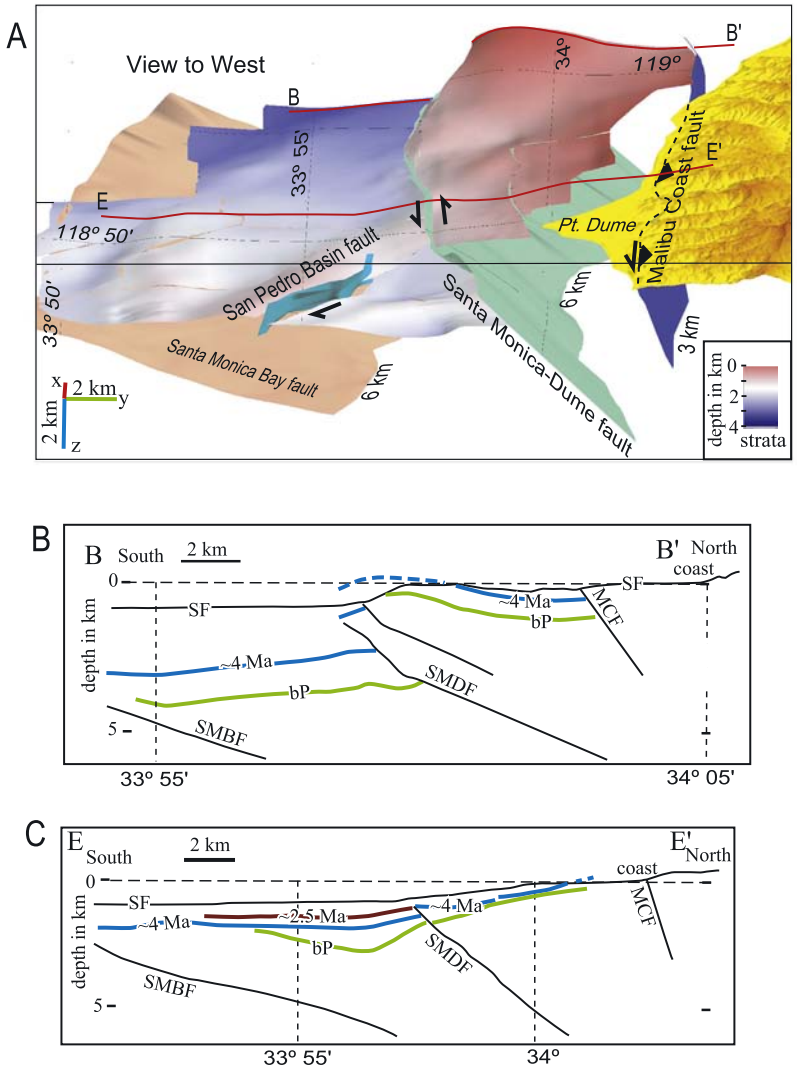


**Figure 10.** (a) View westward from 15° above horizontal of north dipping faults and a bend in the Santa Monica–Dume fault. The back edge is cut along B-B′ (Figure 6). Onshore Malibu Coast fault in foreground is from SCEC CFM. The stratigraphic horizon is 4 ± 1 Ma. The structural relief of this horizon increases westward along the WNW striking Dume segment. Growth of structural relief in the background, along B-B' (Figure 10b), is mainly by fault slip on the Santa Monica–Dume fault, and folding close to it. Faulting and folding close to that fault is insignificant along E-E′ (Figure 10c), however, and structural relief growth is by regional tilting of a broad fold limb above the underlying blind Santa Monica Bay fault, and by reverse-left oblique displacement on the onshore Malibu Coast fault. Blind displacement on the deep blind fault and shortening across and near the Malibu Coast fault both increase eastward. SF, Seafloor; bP, base Pliocene; SMBF, Santa Monica Bay fault; SMDF, Santa Monica–Dume fault; MCF, Malibu Coast fault.

ing increasing westward along the Dume segment and eastward along the Malibu Coast fault (Figure 9). This relation is not consistent with slip partitioning between the two faults, because both are strike slip with oblique slip in restraining segments, rather than the steeper fault being strike slip and the moderately dipping fault being a thrust.

### 7.2.3. Modeling the Restraining Domain Between Fault Bends

[39] The effects of cumulative left-lateral slip are examined here by comparing fault strike and structural relief along the restraining segment on the Santa Monica–Dume fault. Structural relief of the ~4 Ma horizon from combined faulting and folding was measured within 2 km of the fault on 36 N-S contiguous 1-km-thick slices of the Gocad volume (Figure 11). Structural relief increases abruptly from km 24, where the restraining segment begins, to km 18. Structural relief continues to increase, but at a lower gradient, to km 15. The 6-km-long maximum gradient in structural relief is equal to our preferred estimate for left-lateral displacement on the fault (Figure 11). Eleven kilometers of accumulated left slip cannot be precluded, however, because the structural relief does increase over that distance. Structural relief steadily decreases west of km 14, as expected from the waning effect of the restraining

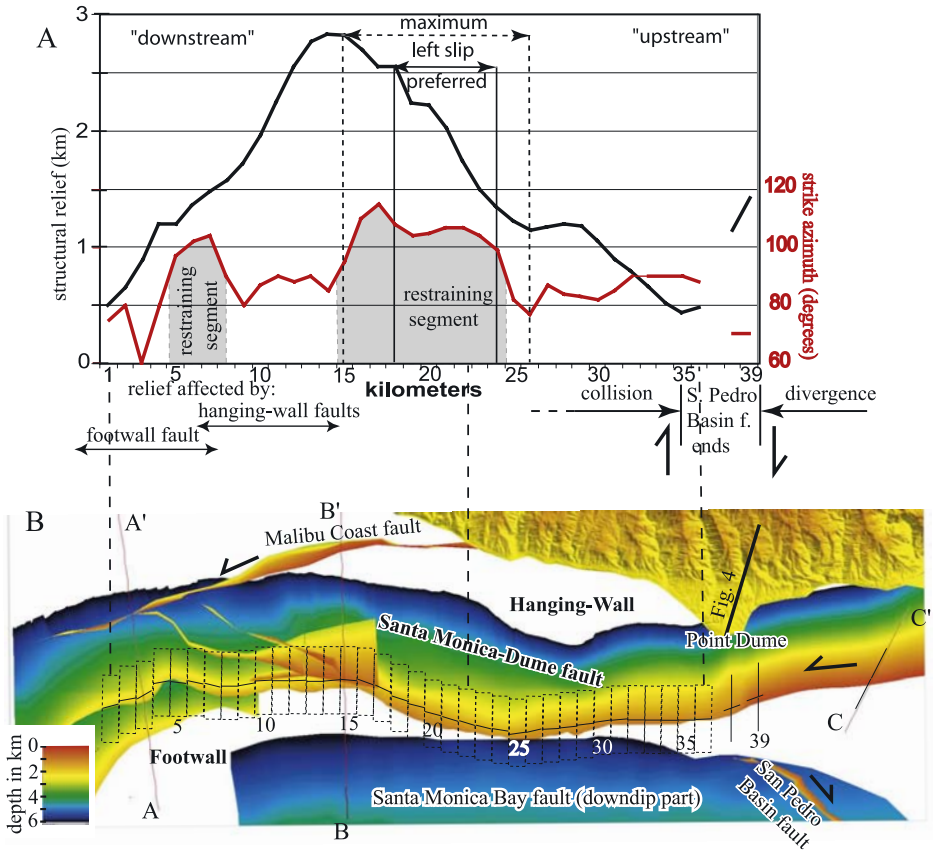


**Figure 11.** Measured, interpreted structural relief plotted against strike of the moderately north dipping, north side-up Santa Monica–Dume fault (SMDF). (a) Structural relief (black) from faulting and folding of ~4 Ma horizon within 2 km either side of the Santa Monica–Dume fault. Relief was measured from 1-km-thick cross-sectional slices, shown in the 4-km-long boxes at the same E-W scale in Figure 11b. Azimuth of the strike of the fault is shown in red in Figure 11a, and is measured at the appropriate depth shown by the labeled line segments, annotated with azimuth, in Figure 11b. Restraining fault segments (azimuths greater than 90) are highlighted in gray. Relative to a fixed footwall, left-lateral displacement brings the hanging wall material into the WNW striking Dume restraining segment at km 24, and structural relief increases westward from that point. Neighboring faults also affect SMDF kinematics, as noted at the bottom of Figure 11a.

segment, west decreasing slip on deeper blind faults, and a releasing component related to clockwise rotation of the hanging wall discussed below.

[40] Predicted structural relief was calculated trigonometrically for a range of horizontal slip directions and by incorporating both the dip and strike of the fault. This modeling assumes that the horizontal component of hanging wall displacement is consistent with a rigid hanging wall block, whereas the vertical component adjusts to fit the morphology of the fault. This structural relief (SR) at any point along the fault can be computed from the geometry of the fault over the slip, assigned to be in the x direction:

$$SR = \int [\sin(\alpha)(x) * \tan(\delta)(x) * dx] \quad (1)$$

where $\alpha$ is the angle between the local slip vector and local fault strike, and $\delta$ is fault dip.

[41] The dip and strike of the fault were measured at each of the cross sections, spaced at 1 km. Given our data, equation (1) can be rewritten

$$SR = \Sigma_i \ 1 \text{ km} * \sin(\alpha_i) * \tan(\delta_i) \quad (2)$$

where the summation is carried out over the slip.

[42] We used equation (2) to generate curves of structural relief between km 11 and 34, and compared the curves to the measured structural relief (Figure 12). This modeling included fault geometry and slip direction east of km 34 because, for larger slips, the hanging wall was transported above the eastern fault. Curves were generated for a range of slip directions and relative rotations across the fault.

[43] The following four criteria are used to match curves: (1) the magnitude of structural relief (the modeling of the single fault can underestimate but not overestimate relief because nonmodeled north dipping faults contribute to

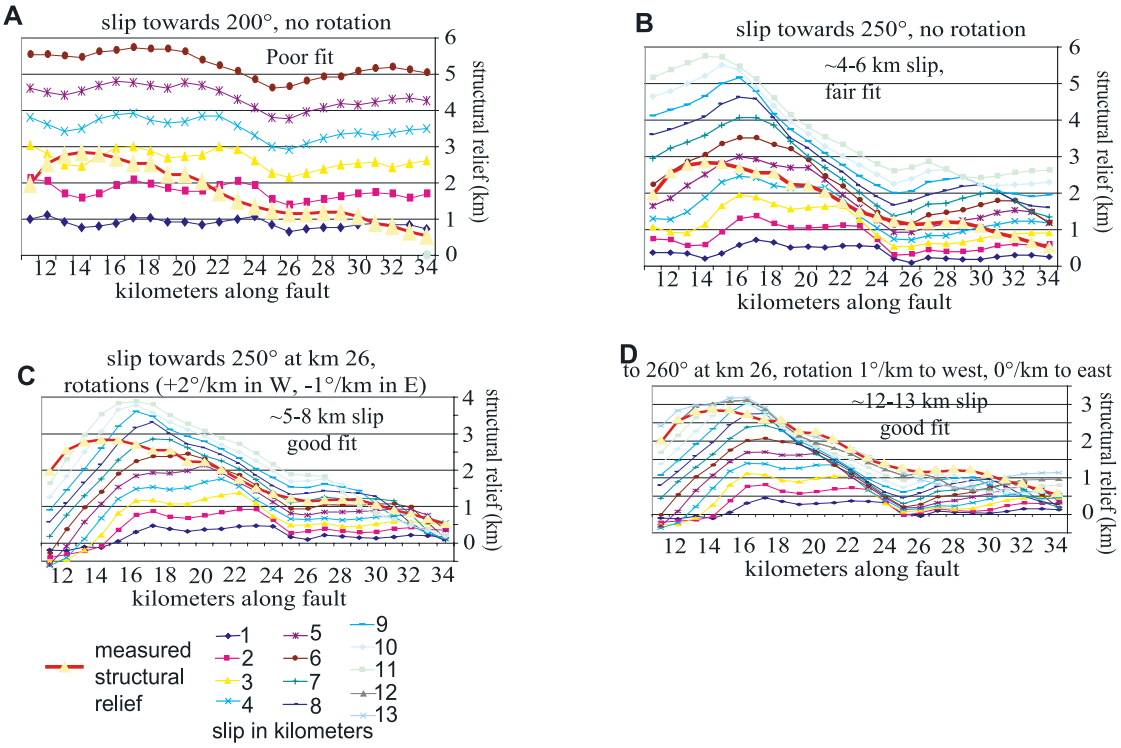


**Figure 12.** Graphs of modeled versus measured structural relief calculated using equation (2). The slip direction of the hanging wall, fault strike, and fault dip are used for each 1 km bin along the fault (Figure 11) to calculate increase in structural relief for rock passing through each bin. The curves for 2, 3 km, etc., slip add the calculated increase in structural relief for each bin 1, 2 km, etc., upstream (east). The heavy red curve is the measured structural relief of the 4 Ma ± 1 m.y. horizon from Figure 11. A discussion of the criteria used to match the curves, and of the best fits among curves is given in paragraph 43. (a) Hanging wall displacement toward 220° along entire fault (no block rotation) gives poor curve matching, so reverse dip slip is not likely along the Dume fault segment. (b) Hanging wall displacement is toward 250° with no rotation, giving a fair curve match for 4 km to 6 km of left-lateral slip. (c) Hanging wall displacement is toward 250° at km 26, increasing (rotating clockwise) by 2°/km to the west, and decreasing 1°/km to the east. The match between modeled and measured relief is good for between 5 km and 8 km of left-lateral displacement. (d) Hanging wall displacement is toward 260° at km 26, increasing (rotating clockwise) by 1°/km to the west, with no relative rotation across the fault to the east. There is a good match between modeled and measured relief for about 12 to 13 km of left-lateral slip.

relief), (2) the length of the change of structural relief along the Dume segment, (3) the gradient of change of structural relief along the Dume segment, and (4) the location of the peak in relief near the west end of the Dume segment.

[44] Four examples of comparison between modeled and measured structural relief curves are discussed here (Figure 12). First, for the simple case of dip slip and no rotation across the Dume segment, the magnitude of modeled structural relief agrees with the measured relief for about 3 km of displacement. The shape of the curves does not match (criteria 2, 3, and 4), however, and therefore dip slip across the Dume segment is unlikely. The second example models slip parallel to the Santa Monica segment, toward 250° (Figure 12b). There is a good match for magnitude and length of change of structural relief for 4 to 6 km of slip, but the gradient of the relief change is flatter for the measured slip than for the modeled slip, and the slope direction does not match at the east end, near the termination of the San Pedro Basin fault. The peak in the measured structural relief is west of the modeled peak, but this may be explained as due to nonmodeled slip on fault splays in this area.

[45] Map restoration and block models indicate that rotation has occurred across the Santa Monica–Dume fault, so that the slip vector changes direction along the fault. Map restoration (Figure 13) discussed below yields 7° of clockwise rotation of the Point Dume block for 5 km of left slip. This rotation changes the slip direction across the Santa Monica–Dume fault by ~32° across 31 km, or 1.03°/km. The block model in Figure 14 includes local clockwise rotation in the footwall south of the Santa Monica segment, so that relative rotation across it is nearly zero. A best fit is produced by use of a clockwise rotation of the slip direction of 2°/km west of km 26 and a counterclockwise rotation of the slip direction of 1°/km east of km 26 (Figure 12c). This greater differential rotation could be related to oroclinal bending of the hanging wall as well as the footwall rotation. The measured and modeled relief has a good fit for magnitude, length, and gradient, for between 5 km and 8 km of left-lateral slip (Figure 12c).

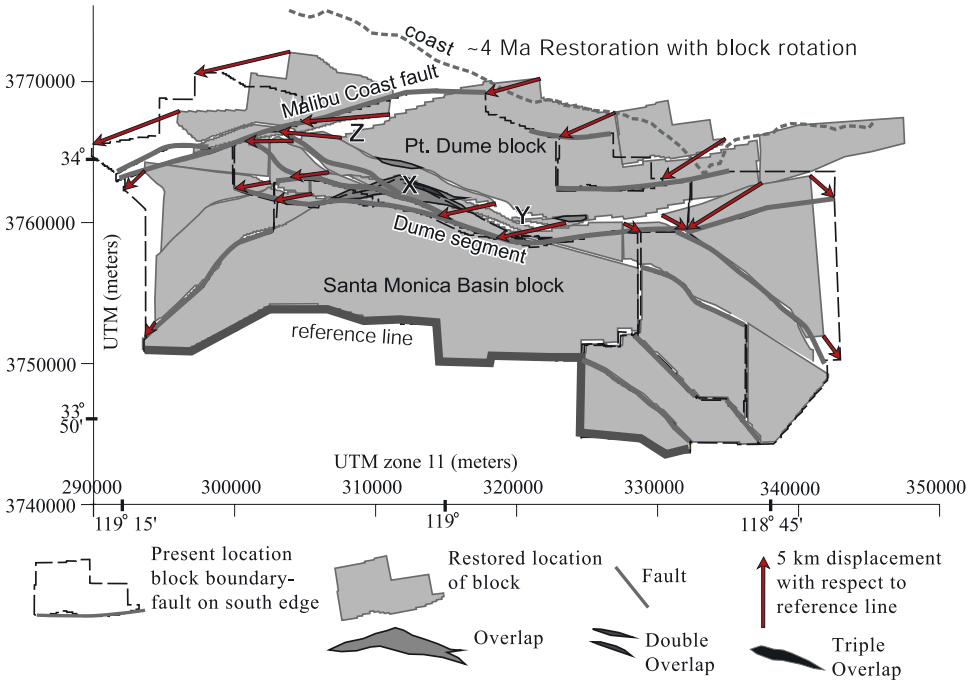


**Figure 13.** Preferred palinspastic restoration using software UNFOLD of the 4 Ma ± 1 m.y. horizon, incorporating 5 km of left separation along the Dume segment. The labeled dashed gray line is the coastline in its present position. The arrows connect the restored block positions to their present positions and represent finite displacement with respect to the reference line. Overlap of restored blocks at "X" (darker grays) indicates areas where we overestimated shortening, and gaps at "Y" (white) indicate underestimated shortening. The deformed state of this map is shown in Figure 2, and faults are labeled there. The 2 km of left separation shown across the Malibu Coast fault is based on modeling discussed in the text and Figure 14. Space problems exist near the intersection of the Dume segment and Malibu Coast fault (at "Z").

[46] Last, slip toward 260° and clockwise rotation of the slip direction of 1°/km west of km 26 produces modeled curves that match the measured curve for all four criteria for left-lateral slip of about 12 to 13 km (Figure 12d). Larger slip than 13 km is unlikely because the structural relief should in that case remain near a maximum for a longer distance "downstream" west of the restraining segment (Figure 9d). Slip is probably less than 13 km because of the nonmodeled effects of fault splays with restraining west-northwest strikes.

[47] This modeling easily explains the abrupt plunges of the anticline that includes Sycamore Knoll (Figure 9a). Doubly plunging folds are present along other strike-slip faults in California and were explained as due to transpression against restraining parts of the fault, including folds in offshore Santa Maria basin [*Sorlien et al.*, 1999a, 1999b], and along the Newport Inglewood fault [*Harding*, 1973; *Wright*, 1991].

### 7.2.4. Retrodeformation of a Digital Horizon Using UNFOLD

[48] We use UNFOLD and map restoration to test which part of the slip range from restraining segment modeling is most likely. Our mapping has produced a 3-D rendering of faults, folding of layers between faults, and vertical separation and horizontal overlap of these layers across faults. We use this information to restore the deformed horizons to their original shapes and relative positions. Maps of fault-bounded domains of the ~4 Ma horizon were restored to a horizontal state with UNFOLD (Figure 13). The flattened digital maps were then assembled with respect to a southern reference line, restoring overlap across reverse-separation faults. This procedure quantifies shortening rather than structural relief.

[49] The map restoration examines how displacement on the Santa Monica–Dume fault relates to displacement on other faults and to block rotation. Five kilometers of left slip along the Dume segment was imposed on the map restoration in Figure 13. This 5 km slip required a 7° clockwise rotation of the Point Dume block to minimize gaps and overlaps in fitting of the unfolded digital maps. Right-lateral slip on two strands of the San Pedro Basin fault is 2 km in this fitting. Left-lateral slip on the Santa Monica segment is about 6 km in the model (Figure 13).

### 7.2.5. Regional Block Model: Left-Lateral Slip and Clockwise Block Rotation

[50] A scaled simplified model of fault-bounded blocks was constructed that includes displacements from quantitative map restoration (Figure 14). The simplified model illustrates the kinematics of block rotations and fault terminations over Santa Monica Bay and nearby land areas. The map view trace of the Santa Monica–Dume fault is concave northward along ~40 km (Figure 14). If displacement was

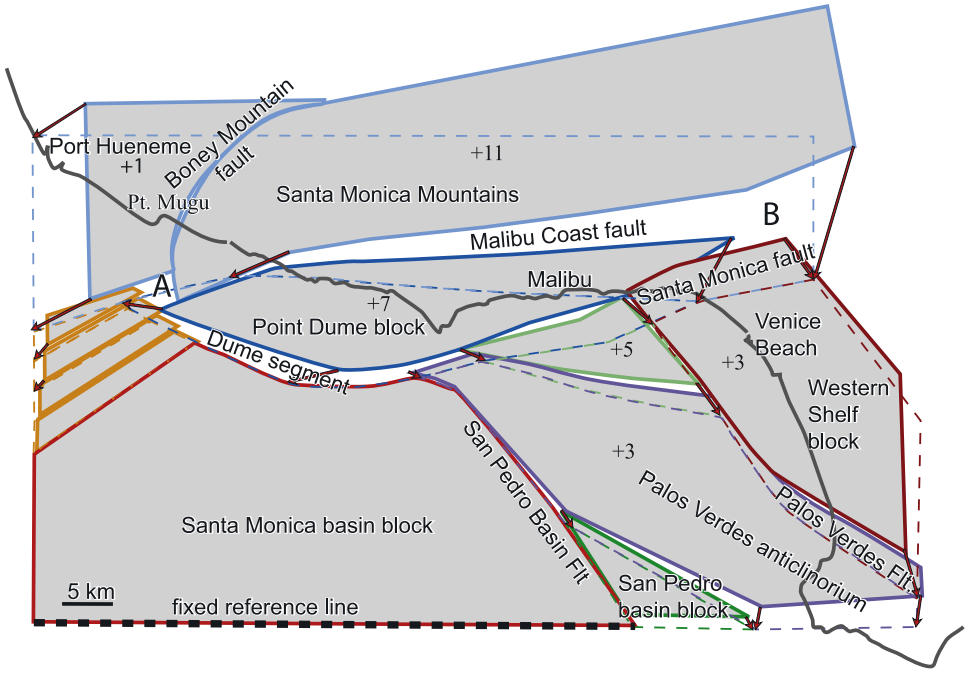


**Figure 14.** Simplified palinspastic restoration of the Santa Monica Mountains and offshore areas to the south. Blocks in their present locations are shown by the dashed polygons. The restored (to about 4 Ma) positions are shown by filled gray polygons with block limits of the same color. Arrows represent displacement with respect to the fixed reference line, connecting restored block corners to the corresponding present position. Where the two figures coincide, displacements are closely similar to those in Figure 13. Gaps between filled polygons represent areas of shortening. The numbers represent degrees of clockwise rotation. Location A represents a space problem at the intersection of the Dume segment with the Malibu Coast fault (the same location as "Z" in Figure 13); location B represents excessive shortening that can also be solved by internal deformation of the large blocks shown here. The larger the relative clockwise rotation of the Santa Monica Mountains, the larger the left-lateral displacement on the faults that bound it to the south and the larger the right-lateral displacement on NW-SE faults that terminate against them. Right-lateral slip is partially absorbed by local rotations so that large velocity discontinuities (space problems) do not exist at fault terminations.

pure left-lateral along this entire length, then the Point Dume block to the north would rotate clockwise relative to the Santa Monica basin block. If the boundary between these blocks were an arc of a circle, then a linear relation would exist between rotation and left-lateral slip, and there would be no gaps or overlaps between domains. The fault exhibits a sharp bend rather than an arc of a circle southwest of Point Dume, however, so that left-lateral displacement causes shortening as well as rotation across the Dume segment (gaps in Figure 14).

[51] The Malibu Coast fault also has both geologic and geometric evidence for left slip, including onshore left canyon deflections or offsets at the fault [*Dibblee*, 1982], and seismic reflection imaging of vertical dip on the offshore fault in the upper 3 km (Figure 5). The fault strike bends more than 20° offshore of Point Mugu (Figures 2b and 9a). East of that bend, vertical and overturned Monterey Formation beds and reverse separations are associated with the west striking onshore Malibu Coast fault zone (Figure 4), including the eastern Los Flores thrust of *Dibblee* [1993]. The onshore fault zone can be considered a restrained domain in the left-lateral Malibu Coast–Santa Cruz Island fault, characterized by left-reverse oblique slip.

[52] If the age of deformation can be inferred, then the bend in the Malibu Coast fault and the along-strike change in shortening can be used to model left-lateral slip. We assert that shortening recorded by middle Miocene strata represents post-Miocene, and possibly post-4 Ma, deformation. Shortening across the Dume segment started about the time of deposition of the ~4 Ma horizon (sections 5.3 and 7.1; Figure 5). Stratal thinning onto folds on geologic sections across the boundary between Los Angeles basin and the Santa Monica Mountains from *Wright* [1991] indicates that shortening started after Miocene time. The use of simple trigonometry demonstrates that almost 9 km of left slip is required to make 3 km of shortening on the restraining side of a 20° bend. Alternatively, this shortening can be explained by ~5° of clockwise rotation of the Santa Monica Mountains with respect to the block between the Santa Monica–Dume fault and Malibu Coast fault. For this estimate, the blocks are pinned at the intersection of the Santa Monica–Dume fault with the Malibu Coast fault ("A" in Figure 14). Because shortening increasing eastward is consistent with rotation, we prefer a composite model that incorporates 2 km of left slip on the Malibu Coast fault and 4° of relative rotation in our restoration.

[53] Current rotations modeled from GPS data can be compared to long-term rotations derived from paleomagnetic data and our block models. The regional block model (Figure 14), which incorporates the restoration of the ~4 Ma horizon (Figure 13), includes 11° of clockwise rotation of the Santa Monica Mountains block with respect to the Santa Monica Basin block, or 2.8°/m.y. since 4 ± 1 m.y. The Santa Monica Mountains block has undergone at least 75° of clockwise rotation since eruption of the 17.4–16.3 Ma Conejo Volcanics there, so long-term average rotation exceeds 4.4°/m.y. [*Kamerling and Luyendyk*, 1979; *McCulloh et al.*, 2002; P. Gans, written communication, 19 October 2004]. The present rate of rotation of the Santa Monica Mountains is 7° ± 1°/m.y., as modeled from GPS data, a little faster than the postvolcanic rate [*Donnellan et al.*, 1993]. The most recent published analysis of modeled GPS data indicates that the Santa Monica Mountains are rotating clockwise 2.4°/m.y. with respect to the San Gabriel Mountains block (*Argus et al.* [2005 p. 20], the "counterclockwise" in their text is an error and should be "clockwise" (D. Argus, written communication, 20 July 2005)). The San Gabriel Mountains block was modeled using GPS data to rotate clockwise at 2.1° ± 0.7°/m.y. with respect to a reference frame that combines motion of Channel Islands to the west and south of Santa Monica basin [*Argus et al.*, 1999]. Therefore the Santa Monica Mountains rotate clockwise about 4.5°/m.y with respect to the Channel Islands reference. If this Channel Islands reference frame did not rotate with respect to the Santa Monica basin block, then the current GPS rotation rate can be compared to our modeled post-~4 Ma rate. The higher GPS rotation rate suggests a higher current rate of left-lateral slip on the Santa Monica–Dume fault than the long-term rate of 1.25 mm/yr used in Figure 13.

[54] The Malibu Coast fault and its left-reverse oblique slip merges with the Santa Monica fault and its left-slip displacement in the near offshore of Santa Monica/Potrero Canyon (Figure 2b). Therefore the onshore Santa Monica fault segment is a left-reverse oblique fault [e.g., *Dolan et al.*, 2000]. Our preferred estimate for left separation on the onshore Santa Monica fault is 8 km since 4 Ma ± 1 m.y. This slip is consistent with the post-8 Ma 15 km left offset of Tarzana Fan (Figure 1a) [*Wright*, 1991]. Additional earlier left-lateral slip occurred across faults separating the wTR from the Los Angeles basin and the Inner Borderland, because basement rocks and Paleogene sedimentary features are left separated by between 32 and 90 km [*Campbell and Yerkes*, 1976; *Truex*, 1976; *Dibblee*, 1982; *Wright*, 1991].

#### 7.2.6. Limitations of the Models

[55] Possible left-oblique reverse slip ranges between 4 and 13 km on the Dume segment (Figures 11 and 12). Five km of left displacement are incorporated in the map restoration because space problems (near "Z" in Figure 13) become severe if, for example, 10 to 13 km of left-lateral slip on the Santa Monica–Dume fault is incorporated. The arcuate Boney Mountain fault [*Dibblee and Ehrenspeck*, 1990] may continue offshore and reduce this space problem (at "A" in Figure 14) [see also *Fisher et al.*, 2005]. The high end of the range of possible slips from the bend modeling in Figure 12d is unlikely.

[56] Errors in our age estimate for the modeled "~4 Ma" horizon of ±25% were discussed above in section 5.3. Errors for our 2 km estimate for left-lateral slip on the Malibu Coast fault could be large. If there were no relative block rotation across that fault, then the fitting of simple rigid blocks across the bend would allow 9 km of left slip. The pattern of shortening across the onshore Malibu Coast fault suggests relative rotation does exist, and the low end of a permissible 1 km to 9 km left-lateral displacement is most reasonable. The Santa Monica–Dume fault becomes mostly blind below the ~4 Ma horizon beneath Hueneme Fan, and therefore we model most of the left-lateral displacement as merging with the Malibu Coast fault (Figure 13). Our preferred estimate for left-lateral displacement west of this merge, 4.5 km, seems high, but is not impossible, for a fault with only 200 m vertical separation of ~4 Ma strata.

## 8. Conclusions

[57] Three main north dipping faults mark the structural front of the western Transverse Ranges in the onshore-offshore area near Los Angeles. The northern one (Malibu Coast fault) is the steepest, the middle one (Santa Monica–Dume fault) dips moderately, and the southern one (Santa Monica Bay fault) is a gently dipping blind fault (Figure 10). The northern and middle faults are both left-lateral in their ENE striking segments, with left-reverse oblique slip in their restraining segments. The Santa Monica Bay fault is interpreted as the carrier of blind thrust displacement at depth. The onshore-offshore Santa Monica–Dume fault is an 80-km-long, reactivated Miocene normal-separation fault, which may explain its moderate dip. This arcuate offshore fault is a kinematically continuous left-lateral fault with a subsidiary reverse component in the Dume restraining segment. It is underlain by the large Miocene low-angle normal-separation Santa Monica Bay fault, and its hanging wall is cut by the left-lateral (west) or left-oblique reverse (east) Malibu Coast fault. High-angle faults with small vertical separations link the Dume segment to the Malibu Coast fault, which in turn is continuous with the Santa Cruz Island fault 20 km west of our study area (Figure 1).

[58] The offshore faults are more geometrically continuous than previously mapped (Figure 1). The modeled left-lateral displacement of 6 km or more on the offshore Santa Monica segment requires it to be linked to the onshore Santa Monica fault. This left-lateral slip is related to clockwise rotation of the Santa Monica Mountains. Continued Holocene left-lateral slip on the onshore Santa Monica fault [*Dolan et al.*, 2000] suggests that clockwise rotation of the Santa Monica Mountains continues today. The San Pedro basin fault and the Palos Verdes fault are active NW striking right-lateral faults that are high angle in at least their upper 1–2 km [*Broderick*, 2006]. These faults branch into WNW striking splays near their intersections with, or terminations near, the E-W Santa Monica Dume fault (Figure 2b).

[59] The newly mapped 3-D geometry of faults and a deformed ~4 Ma horizon allows qualitative and quantitative modeling of displacement across the Santa Monica–Dume fault. A range of models explains the growth of structural relief and shortening through bends of this arcuate fault. These combined analyses produce estimates of 5 +8/−1 km of left-lateral separation in the last 4 (±1) m.y. along the Dume segment, and 8 +18/−2 km left separation

across the onshore Santa Monica fault. The estimated displacements are consistent with 7°of relative clockwise rotation of the Point Dume block, and 11° of clockwise rotation of the Santa Monica Mountains block. Post-Miocene subsidence of the Santa Monica basin in the footwall of the Santa Monica–Dume fault approaches 0.8 mm/yr. Growth of structural relief is substantially larger than surface or rock uplift (with respect to sea level) if this subsidence is ongoing. Thus displacements on blind faults are likely to be greater than would be estimated using rock or surface uplift alone [e.g., *Pinter et al.*, 2003]. Increase of structural relief of ~1 mm/yr suggests a blind thrust component is present on the underlying Santa Monica Bay fault, and possibly on downdip projections of the Santa Monica–Dume fault. This blind slip increases from west to east. Thus N-S shortening is accommodated both by conjugate strike-slip faulting with tectonic escape, and by crustal thickening [*Walls et al.*, 1998; *Argus et al.*, 1999].

[60] **Acknowledgments.** The efforts of Tom Wright and David Okaya made industry data available to SCEC researchers. Other industry sources provided additional seismic reflection data. Drew Mayerson and others at the U.S. Minerals Management Service released the Digicon data. Mike Fisher, Bill Normark, and Ray Sliter provided data used in mapping the southeast part of the study area. Jean-Pierre Gratier provided the UNFOLD software and advice on its use. Bruce Luyendyk provided guidance to Kris Broderick as his thesis advisor. Marie-Helene Cormier provided the inset for Figure 8 and edited the manuscript, as did Art Sylvester. Associate Editor Kelin Wang and reviewers Ken Hudnut, Tom Brocher, and anonymous provided detailed comments that resulted in a more accessible paper of more global interest. This research was supported by the Southern California Earthquake Center. SCEC is funded by NSF Cooperative Agreement EAR-0106924 and USGS Cooperative Agreement 02HQAG0008. The SCEC contribution number for this paper is 846. It was also supported by USGS-NEHRP, USDI/USGS 03HQGR0048 and USDI/USGS 02HQGR0013. Institute for Crustal Studies contribution 794.

## References

Affolter, T., and J.-P. Gratier (2004), Map view retrodeformation of an arcuate fold-and-thrust belt: The Jura case, *J. Geophys. Res.*, *109*, B03404, doi:10.1029/2002JB002270.

Anderson, E. M. (1951), *The Dynamics of Faulting*, 199 pp., Oliver and Boyd, White Plains, N. Y.

Argus, D. F., M. B. Heflin, A. Donnellan, F. H. Webb, D. Dong, K. J. Hurst, D. C. Jefferson, G. A. Lyzenga, M. M. Watkins, and J. F. Zumberge (1999), Shortening and thickening of metropolitan Los Angeles measured and inferred by using geodesy, *Geology*, *27*, 703–706.

Argus, D. F., M. B. Heflin, G. Peltzer, F. Crampé, and F. H. Webb (2005), Interseismic strain accumulation and anthropogenic motion in metropolitan Los Angeles, *J. Geophys. Res.*, *110*, B04401, doi:10.1029/2003JB002934.

Atwater, T. (1989), Plate tectonic history of the northeast Pacific and western North America, in *The Geology of North America*, vol. N, *The Eastern Pacific Ocean and Hawaii*, edited by E. L. Winterer, D. M. Hussong, and R. W. Decker, pp. 21–72, Geol. Soc. of Am., Boulder, Colo.

Atwater, T., and J. M. Stock (1998), Pacific-North America plate tectonics of the Neogene southwestern United States—An update, *Int. Geol. Rev.*, *40*, 375–402.

Bailey, T. L., and R. H. Jahns (1954), Geology of the Transverse Range Province, Southern California, in *Geology of Southern California*, chapter II, *Geology of the Natural Provinces*, *Calif. Div. Mines Bull.*, *170*, 83–106.

Birkeland, P. W. (1972), Late Quaternary eustatic seal-level changes along the Malibu coast, Los Angeles County, California, *J. Geol.*, *80*, 432–448.

Blake, G. H. (1991), Review of the Neogene biostratigraphy and stratigraphy of the Los Angeles Basin and implications for basin evolution, in *Active Margin Basins*, edited by K. T. Biddle, *AAPG Mem.*, *52*, 135–184.

Bohannon, R. G., J. V. Gardner, and R. W. Sliter (2004), Holocene to Pliocene tectonic evolution of the region offshore of the Los Angeles urban corridor, southern California, *Tectonics*, *23*, TC1016, doi:10.1029/2003TC001504.

Broderick, K. G. (2006), Giant blind thrust faults beneath the Palos Verdes Hills and western Los Angeles Basin, California: Mapping with seismic reflection and deep drilling data, M. S. thesis, 68 pp., Univ. of Calif., Santa Barbara.

Burdick, D. J., and W. C. Richmond (1982), A summary of geologic hazards for proposed OCS oil and gas lease sale 68, southern California, *U. S. Geol. Surv. Open File Rep., 82-33*.

California Division Oil, Gas, and Geothermal Resources (1992), California oil and gas fields, vol. II, Southern, central coastal, and offshore California, *Publ. TR11*, Sacramento.

Campbell, R. H., and R. F. Yerkes (1976), Cenozoic evolution of the Los Angeles basin area—Relationship to plate tectonics, in *Aspects of the Geological History of the California Borderland*, edited by D. G. Howell, *Misc. Publ. 24*, pp. 541–558, Pac. Sect., Am. Assoc. of Pet. Geol., Bakersfield, Calif.

Cande, S. C., C. A. Raymond, J. Stock, and W. F. Haxbe (1995), Geophysics of the Pitman Fracture Zone and Pacific-Antarctic plate motion during the Cenozoic, *Science*, *270*, 947–951.

Clark, D. H., N. T. Hall, D. H. Hamilton, and R. G. Heck (1991), Structural analysis of late Neogene deformation in the central offshore Santa Maria Basin, California, *J. Geophys. Res.*, *96*, 6435–6457.

Cormier, M.-H., et al. (2006), North Anatolian Fault in the Gulf of Izmit (Turkey): Rapid vertical motion in response to minor bends of a non-vertical continental transform, *J. Geophys. Res.*, *111*, B04102, doi:10.1029/2005JB003633.

Cowgill, E., A. Yin, J. R. Arrowsmith, W. X. Feng, and Z. Shuanhong (2004), The Akato Tagh bend along the Altyn Tagh fault, northwest Tibet. 1: Smoothing by vertical-axis rotation and the effect of topographic stresses on bend-flanking faults, *Geol. Soc. Am. Bull.*, *116*, 1423–1442, doi:10.1130/B25359.1.

Crouch, J. K., and J. Suppe (1993), Late Cenozoic tectonic evolution of the Los Angeles basin and inner California borderland: A model for core complex-like crustal extension, *Geol. Soc. Am. Bull.*, *105*, 1415–1434.

Crowell, J. C. (1974), Origins of late Cenozoic basins in southern California, in *Tectonics and Sedimentation*, edited by W. R. Dickinson, *Spec. Publ. SEPM Soc. Sediment. Geol.*, *22*, 190–204.

Crowell, J. C. (1979), The San Andreas fault system through time, *J. Geol. Soc. London*, *136*, 293–302.

Dartnell, P., and J. V. Gardner (1999), Sea-floor images and data from multibeam surveys in San Francisco Bay, southern California, Hawaii, the Gulf of Mexico, and Lake Tahoe, California-Nevada, *U. S. Geol. Surv. Digital Data Ser.,* DDS-55 version 1.0.

Davis, T. L., and J. S. Namson (1994), A balanced cross-section of the 1994 Northridge earthquake, southern California, *Nature*, *372*, 167–169.

Davis, T. L., J. Namson, and R. F. Yerkes (1989), A cross section of the Los Angeles Area: Seismically active fold and thrust belt, the 1987 Whittier Narrows earthquake, and earthquake hazard, *J. Geophys. Res.*, *94*, 9644–9664.

Dibblee, T. W., Jr. (1982), Geology of the Santa Monica Mountains and Simi Hills, southern California, in *Geology and Mineral Wealth of the California Transverse Ranges*, edited by D. L. Fife and J. A. Minch, pp. 94–130, South Coast Geol. Soc., Santa Ana, Calif.

Dibblee, T. W., Jr. (1992), Geologic map of the Topanga and Canoga Park (south 1/2) quadrangles, Los Angeles County, California, *Map DF-35*, scale 1:24000, edited by H. E. Ehrenspeck, Dibblee Geol. Found., Santa Barbara, Calif.

Dibblee, T. W., Jr. (1993), Geologic map of the Malibu Beach quadrangle, Los Angeles County, California, *Map DF-47*, scale 1:24000, edited by H. E. Ehrenspeck and W. L. Bartlett, Dibblee Geol. Found., Santa Barbara, Calif.

Dibblee, T. W., Jr., and H. E. Ehrenspeck (1990), Geologic Map of the Point Mugu and Triunfo Pass quadrangles, Ventura and Los Angeles counties, California, *Map DF-29*, scale 1:24000, Dibblee Geol. Found., Santa Barbara, Calif.

Dibblee, T. W., Jr., and H. E. Ehrenspeck (1993), Geologic map of the Point Dume quadrangle, Los Angeles and Ventura counties, California, *Map DF-48*, scale 1:24000, Dibblee Geol. Found., Santa Barbara, Calif.

Dolan, J. F., K. E. Sieh, T. K. Rockwell, R. S. Yeats, J. Shaw, J. Suppe, G. J. Huftile, and E. M. Gath (1995), Prospects for larger or more frequent earthquakes in the Los Angeles metropolitan region, *Science*, *267*, 199–205.

Dolan, J. F., K. E. Sieh, and T. K. Rockwell (2000), Late Quaternary activity and seismic potential of the Santa Monica fault system, Los Angeles, California, *Geol. Soc. Am. Bull.*, *112*, 1559–1581.

Donnellan, A., B. H. Hager, R. W. King, and T. A. Herring (1993), Geodetic measurement of deformation in the Ventura Basin region, southern California, *J. Geophys. Res.*, *98*, 21,727–21,739.

Fisher, M. A., W. R. Normark, R. G. Bohannon, R. W. Sliter, and A. J. Calvert (2003), Geology of the continental margin beneath Santa Monica Bay, southern California, from seismic reflection data, *Bull. Seismol. Soc. Am.*, *93*, 1955–1983.

Fisher, M. A., V. E. Langenheim, C. C. Sorlien, M. J. Kamerling, P. Dartnell, R. W. Sliter, G. R. Cochrane, and F. L. Wong (2005), Recent deformation along the offshore Malibu Coast, Dume, and related faults west of Point Dume, southern California, *Bull. Seismol. Soc. Am.*, *95*, 2486–2500, doi:10.1785/0120050042.

Gratier, J.-P., B. Guillier, A. Delorme, and F. Odonne (1991), Restoration and balance of a folded and faulted surface by best-fitting of finite elements: Principle and applications, *J. Struct. Geol.*, *13*, 111–115.

Gratier, J.-P., T. Hopps, C. C. Sorlien, and T. Wright (1999), Recent crustal deformation in southern California deduced from the restoration of folded and faulted strata, *J. Geophys. Res.*, *104*, 4887–4899.

Harding, T. P. (1973), Newport-Inglewood trend, California—An example of wrenching style of deformation, *Am. Assoc. Pet. Geol. Bull.*, *57*, 96–116.

Harding, T. P. (1990), Identification of wrench faults using subsurface structural data: Criteria and pitfalls, *AAPG Bull.*, *74*, 1590–1609.

Hauksson, E., and G. V. Saldivar (1986), The 1930 Santa Monica and the 1979 Malibu, California, earthquakes, *Bull. Seismol. Soc. Am.*, *76*, 1542–1559.

Huftile, G. J., and R. S. Yeats (1996), Deformation rates across the Placerita (Northridge $M_w$ = 6.7 aftershock zone) and Hopper Canyon segments of the western Transverse Ranges deformation belt, *Bull. Seismol. Soc. Am.*, *86*, 3–18.

Jennings, C. W. (1994), Fault activity map of California and adjacent areas with locations and ages of recent volcanic eruptions, *Geol. Data Map 6*, scale 1:750,000, Calif. Div. Mines and Geol., Sacramento.

Junger, A., and H. C. Wagner (1977), Geology of the Santa Monica and San Pedro Basins, California continental borderland, *U. S. Geol. Surv. Misc. Field Stud. Map, MF-820*, 10 pp., 5 plates, scale 1:250,000.

Kamerling, M. J., and B. P. Luyendyk (1979), Tectonic rotations of the Santa Monica Mountains region western Transverse Ranges, California, suggested by paleomagnetic vectors, *Geol. Soc. Am. Bull.*, *90*, 331–337.

Kamerling, M., and B. P. Luyendyk (1985), Paleomagnetism and Neogene tectonics of the northern Channel Islands, California, *J. Geophys. Res.*, *90*, 12,485–12,502.

Keller, E. A., and H. A. Loaiciga (1993), Fluid-pressure induced seismicity at regional scales, *Geophys. Res. Lett.*, *20*, 1683–1686.

Keller, E. A., D. L. Johnson, D. L. Laduzinsky, D. B. Seaver, and T. L. Ku (2000), Tectonic geomorphology of active folding over buried reverse faults: San Emigdio Mountain Front, southern San Joaquin Valley, California, *Geol. Soc. Am. Bull.*, *112*, 86–97.

Legg, M. R. (1991), Developments in understanding the tectonic evolution of the California Continental Borderland, in *Shepard Commemorative Volume, From Shoreline to Abyss*, edited by R. H. Osborne, *Spec. Publ. SEPM Soc. Sediment. Geol.*, *46*, 291–312.

Legg, M. R., M. J. Kamerling, and R. D. Francis, (2004), Termination of strike-slip faults at convergence zones within continental transform boundaries: Examples from the California Continental Borderland, in *Vertical Coupling and Decoupling in the Lithosphere*, edited by J. Grocott et al., *Geol. Soc. Spec. Publ.*, *227*, 65–82.

Lettis, W. R., and K. L. Hanson (1991), Crustal strain partitioning: Implications for seismic-hazard assessment in western California, *Geology*, *19*, 559–562.

Lonsdale, P. (1991), Structural patterns of the Pacific floor offshore of peninsular California, Gulf and Peninsular Provinces of the Californias, in *Gulf and Peninsular Provinces of the Californias*, edited by P. Dauphin, G. Ness, and B. Simoneit, *AAPG Mem.*, *47*, 87–126.

Mallet, J. L. (1997), Discrete modeling for natural objects, *Math. Geol.*, *29*, 199–219.

McCulloh, T. H., R. J. Fleck, R. E. Denison, L. A. Beyer, and R. G. Stanley (2002), Age and tectonic significance of volcanic rocks in the northern Los Angeles Basin, California, *U.S. Geol. Surv. Prof. Pap.*, *1669*, 24 pp.

Meade, B. J., and B. H. Hager (2005), Block models of crustal motion in southern California constrained by GPS measurements, *J. Geophys. Res.*, *110*, B03403, doi:10.1029/2004JB003209.

Meigs, A., N. Brozovic, and M. L. Johnson (1999), Steady, balanced rates of uplift and erosion of the Santa Monica Mountains, California, *Basin Res.*, *11*, 59–73.

Moore, G. W., and D. S. McCulloch (1975), Acoustic-reflection profiles M/V Oil City June 1969 offshore southern California, *U. S. Geol. Surv. Open File Rep., 75-347*.

Namson, J., and T. Davis (1992), Late Cenozoic thrust ramps of southern California, final report for 1991 contract, South. Calif. Earthquake Center, Los Angeles. (Available at http://www.davisnamson.com/downloads/index.htm)

Nardin, T. R., and T. L. Henyey (1978), Pliocene-Pleistocene diastrophism of Santa Monica and San Pedro shelves, California Continental Borderland, *AAPG Bull.*, *62*, 247–272.

Nicholson, C., C. C. Sorlien, T. Atwater, J. C. Crowell, and B. P. Luyendyk (1994), Microplate capture, rotation of the Western Transverse Ranges, and initiation of the San Andreas transform as a low-angle fault system, *Geology*, *22*, 491–495.

Normark, W. R., D. J. Piper, and R. N. Hiscott (1998), Sea level controls on the textural characteristics of the Hueneme and associated submarine fan systems, Santa Monica basin, California, *Sedimentology*, *45*, 53–70.

Normark, W. R., S. Baher, and R. Sliter (2004), Late Quaternary sedimentation and deformation in Santa Monica and Catalina Basins, in *Geology and Tectonics of Santa Catalina Island and the California Continental Borderland*, edited by M. R. Legg, P. Davis, and E. Gath, *1004 Field Trip Guideb. 32*, pp. 291–318, South Coast Geol. Soc., Santa Ana, Calif.

Okay, A. I., O. Tuysuz, and S. Kaya (2004), From transpression to transtension: Changes in morphology and structure around a bend on the North Anatolian Fault in the Marmara region, *Tectonophysics*, *391*, 259–282.

Pinter, N., C. C. Sorlien, and A. T. Scott (2003), Fault-related fold growth and isostatic subsidence, California Channel Islands, *Am. J. Sci.*, *303*, 300–318.

Plesch, A., and J. H. Shaw (2002), SCEC 3D community fault model for southern California, *Eos Trans. AGU*, *83*(47), Fall Meeting Suppl., Abstract S21A-0966.

Rivero, C., J. H. Shaw, and K. Mueller (2000), Oceanside and Thirtymile Bank blind thrusts: Implications for earthquake hazards in coastal southern California, *Geology*, *28*, 891–894.

Schneider, C. L., C. Hummon, R. S. Yeats, and G. L. Huftile (1996), Structural evolution of the northern Los Angeles basin, California, based on growth strata, *Tectonics*, *15*, 341–355.

Scholz, C. H. (2002), *The Mechanics of Earthquakes and Faulting*, 2nd ed., 471 pp., Cambridge Univ. Press, New York.

Scientists of U. S. Geological Survey and Southern California Earthquake Center (1994), The magnitude 6.7 Northridge, California earthquake of 17 January, 1994, *Science*, *266*, 389–397.

Seeber, L., and C. C. Sorlien (2000), Listric thrusts in the western Transverse Ranges, California, *Geol. Soc. Am. Bull.*, *112*, 1067–1079.

Seeber, L., O. Emre, M.-H. Cormier, C. C. Sorlien, C. M. G. McHugh, A. Polonia, N. Ozer, N. Cagatay, and the Team of the 2000 R/V *Urania* Cruise in the Marmara Sea (2004), Uplift and subsidence from oblique slip: The Ganos-Marmara bend of the north Anatolian transform, western Turkey, *Tectonophysics*, *391*, 239–258, doi:10.1016/j.tecto.2004.07.015.

Shaw, J. H., and J. Suppe (1994), Active faulting and growth folding in the eastern Santa Barbara Channel, California, *Geol. Soc. Am. Bull.*, *106*, 607–626.

Shaw, J. H., and J. Suppe (1996), Earthquake hazards of active blind-thrust faults under the central Los Angeles basin, California, *J. Geophys. Res.*, *101*, 8623–8642.

Shaw, J. H., R. E. Bischke, and J. Suppe (1994), Relationships between folding and faulting in the Loma Prieta epicentral zone: Strike-slip fault-bend folding, in *The Loma Prieta, California Earthquake of October 17, 1989; Earthquake Occurrence*, edited by R. W. Simpson, *U. S. Geol. Surv. Prof. Pap.*, *1550-F*, F3–F21.

Shen, Z.-K., D. C. Agnew, and R. W. King (2003), The SCEC crustal motion map, version 3.0, South. Calif. Earthquake Center, Los Angeles. (Available at http://epicenter.usc.edu/cmm3/)

Sibson, R. H. (1995), Selective fault reactivation during basin inversion: Potential for fluid redistribution through fault-valve action, in *Basin Inversion*, edited by J. G. Buchanan and P. G. Buchanan, *Geol. Soc. Spec. Publ.*, *88*, 3–19.

Sliter, R. W., W. R. Normark, and C. E. Gutmacher (2005), Multichannel seismic-reflection data acquired off the coast of southern California–Part A 1997, 1998, 1999, and 2000, *U.S. Geol. Surv. Open File Rep., 2005-1084*. (Available at http://pubs.usgs.gov/of/2005/1084/index.html)

Sorlien, C. C., M. J. Kamerling, and D. Mayerson (1999a), Block rotation and termination of the Hosgri strike-slip fault system, California, from 3-D map restoration, *Geology*, *27*, 1039–1042.

Sorlien, C. C., C. Nicholson, and B. P. Luyendyk (1999b), Miocene extension and post-Miocene transpression offshore of south-central California, in *Evolution of Sedimentary Basins/Onshore Oil and Gas Investigations—Santa Maria Province*, edited by M. A. Keller, *U. S. Geol. Surv. Bull., 1995*, chapter Y, 38 pp, 1 plate.

Sorlien, C. C., M. J. Kamerling, K. G. Broderick, and L. Seeber (2003), Structure and kinematics along the thrust front of the Transverse Ranges: 3D digital mapping of active faults in Santa Monica Bay using reflection, well, and earthquake data: Collaborative research with University of California, Santa Barbara, and Columbia University, Final Technical Report to U. S. Geological Survey NEHRP 02HQGR0013, 15 pp., U. S. Geol. Surv., Reston, Va.

Sorlien, C. C., K. G. Broderick, R. Sliter, M. Fisher, W. Normark, L. Seeber, and M. J. Kamerling (2004), Digital 3D mapping of active faults beneath Santa Monica Bay, basin modeling, and strain partitioning: Collaborative Research UCSB and LDEO, Final Report to U.S. Geological Survey NEHRP, contract 03-HQGR-0048, 21 pp., U. S. Geol. Surv., Reston, Va.

Stierman, D. J., and W. L. Ellsworth (1976), Aftershocks of the February 21, 1973 Point Mugu, California earthquake, *Bull. Seismol. Soc. Am.*, *66*, 1931–1952.

Sylvester, A. G. (1988), Strike-slip faults, *Geol. Soc. Am. Bull.*, *100*, 1666–1703.

ten Brink, U. S., J. Zhang, T. M. Brocher, D. A. Okaya, K. D. Klitgord, and G. S. Fuis (2000), Geophysical evidence for the evolution of the California Inner Continental Borderland as a metamorphic core complex, *J. Geophys. Res.*, *105*, 5835–5857.

Truex, J. N. (1976), Santa Monica and Santa Ana Mountains-relation to Oligocene Santa Barbara basin, *AAPG Bull.*, *60*, 65–86.

Tsutsumi, H., R. S. Yeats, and G. J. Huftile (2001), Late Cenozoic tectonics of the northern Los Angeles fault system, California, *Geol. Soc. Am. Bull.*, *113*, 454–468.

Vedder, J. G. (1990), Maps of California Continental Borderland showing compositions and ages of samples acquired between 1968 and 1979, *U.S. Geol. Surv. Misc. Field Stud. Map*, *MF-2122*.

Vedder, J. G., H. G. Greene, S. H. Clarke, and M. P. Kennedy (1986), Geologic map of the mid-southern California continental margin, scale 1:250,000, Calif. Dep. of Mines and Geol., Sacramento.

Walls, C., T. Rockwell, K. Mueller, Y. Bock, S. Williams, J. Pfanner, J. Dolan, and P. Fang (1998), Escape tectonics in the Los Angeles metropolitan region and implications for seismic risk, *Nature*, *394*, 356–360.

Wright, T. L. (1991), Structural geology and tectonic evolution of the Los Angeles Basin, California, in *Active Margin Basins*, edited by K. T. Biddle, *AAPG Mem.*, *52*, 35–134.

Yeats, R. S. (1976), Extension versus strike-slip origin of the southern California Borderland, in *Aspects of the Geological History of the California Borderland, Misc. Pub. 24*, edited by D. G. Howell, pp. 455–485, Pac. Sect., Am. Assoc. of Pet. Geol., Bakersfield, Calif.

Yeats, R. S. (2004), Tectonics of the San Gabriel Basin and surroundings, southern California, *Geol. Soc. Am. Bull.*, *116*, 1158–1182, doi:10.1130/B25346.1.

Yeats, R. S., K. Sieh, and C. R. Allen (1996), *The Geology of Earthquakes*, 568 pp., Oxford Univ. Press, New York.

K. G. Broderick, ExxonMobil Exploration Co., 233 Benmar Dr., Houston, TX 77060, USA.

M. J. Kamerling, Venoco Inc., 6267 Carpinteria Ave. Suite 100, Carpinteria, CA 93013, USA.

L. Seeber, Lamont-Doherty Earth Observatory, Columbia University, Palisades, NY 10964-8000, USA.

C. C. Sorlien, Institute for Crustal Studies, University of California, Santa Barbara, CA 93106, USA. (chris@crustal.ucsb.edu)